8
Functionally Graded Piezoelectric Material Systems – A Multiphysics Perspective

Wilfredo Montealegre Rubio, Sandro Luis Vatanabe, Gláucio Hermogenes Paulino, and Emílio Carlos Nelli Silva

8.1
Introduction

Functionally graded materials (FGMs) possess continuously graded properties and are characterized by spatially varying microstructures created by nonuniform distributions of the reinforcement phase as well as by interchanging the role of reinforcement and matrix (base) materials in a continuous manner. The smooth variation of properties may offer advantages such as local reduction of stress concentration and increased bonding strength [1–3].

Standard composites result from the combination of two or more materials, usually resulting in materials that offer advantages over conventional materials. At the macroscale observation, traditional composites (e.g., laminated) exhibit a sharp interface among the constituent phases that may cause problems such as stress concentration and scattering (if a wave is propagating inside the material), among others. However, a material made using the FGM concept would maintain some of the advantages of traditional composites and alleviate problems related to the presence of sharp interfaces at the macroscale. The design of the composite material itself is a difficult task, and the design of a composite where the properties of its constituent materials change gradually in the unit cell domain is even more complex.

There are two ways to design FGM composites: macro- and microscale approach. In macroscale approach, the conventional piezoelectric active element is replaced by a functionally graded piezoelectric material. Therefore, all or some of the properties (piezoelectric, dielectric, or elastic properties) vary along a specific direction, usually along its thickness, based on a specific gradation function [4–8]. In microscale approach, composites can be modeled by a unit cell with infinitesimal dimensions, which is the smallest structure that is periodic in the composite. By changing the volume fraction of the constituents, the shape of the inclusions, or even the topology of the unit cell, we can obtain different effective properties for the composite material [9]. The calculation of effective properties is necessary to obtain its performance. This can be achieved by applying the homogenization method that plays an important role in the design method.

Advanced Computational Materials Modeling: From Classical to Multi-Scale Techniques.
Edited by Miguel Vaz Júnior, Eduardo A. de Souza Neto, and Pablo A. Munoz-Rojas

ISBN: 978-3-527-32479-8

This chapter is organized as follows. In Section 8.2, a brief introduction about piezoelectricity is presented. In Section 8.3, the concept of FGM is introduced. In Section 8.4, the formulation of the finite element method (FEM) for graded piezoelectric structures is presented, and in Section 8.5 the influence of property scale in piezotransducer performance is described, aiming at ultrasonic applications. The influence of microscale is discussed in Section 8.6, including a brief description of homogenization method. Finally, in Section 8.7, concluding remarks are provided.

8.2 Piezoelectricity

The piezoelectric effect, according to the original definition of the phenomenon discovered by Jacques and Pierre Curie brothers in 1880 [10], is the ability of certain crystalline materials to develop an electric charge that is proportional to a mechanical stress. Thus, piezoelectricity is an interaction between electrical and mechanical systems. The direct piezoelectric effect, the development of an electric charge upon the application of a mechanical stress, is described as [11]

$$P_i = d_{ijk} T_{jk} \tag{8.1}$$

where P_i is a component of the electric polarization (charge per unit area), d_{ijk} are the components of piezoelectric coupling coefficient, and T_{jk} are components of the applied mechanical stress. The converse effect, the development of a mechanical strain upon the application of an electric field to the piezoelectric, is described by Nye [11]:

$$S_{ij} = d_{ijk} E_k \tag{8.2}$$

where S_{ij} is the strain produced and E_k is the applied electric field. In both cases, the piezoelectric coefficients d_{ijk} are numerically identical.

The piezoelectric effect is strongly linked to the crystal symmetry. Piezoelectricity is limited to 20 of the 32 crystal classes. The crystals that exhibit piezoelectricity have one common feature: the absence of a center of symmetry within the crystal. This absence of symmetry leads to polarity, the one-way direction of the charge vector. Most of the important piezoelectric materials are also ferroelectric [10]. The piezoelectric effect occurs naturally in several materials (quartz, tourmaline, and Rochelle salt), and can be induced in other polycrystalline materials; for example, the barium titanate ($BaTiO_3$), polyvinylidene fluoride (PVDF), and the lead zirconate titanate (PZT). Nevertheless, in these nonnatural materials, the piezoelectric effect must be induced through a process of electric polarization [12]. Basically, in the polarization process, the piezoelectric material is heated to an elevated temperature while in the presence of a strong DC field (usually higher than 2000 V mm^{-1}). This polarizes the ceramic (aligning the molecular dipoles of the ceramic in the direction of the applied field) and provides it with piezoelectric properties.

The piezoelectric effect can be described using a set of basic equations. The constitutive relations for piezoelectric media give the coupling between the mechanical and the electrical parts of a piezoelectric system. Thus, the equations of linear piezoelectricity, as given in the IEEE Standard on Piezoelectricity [13], and by using Einstein's summation convention (see also Ref. [14]), can be written as

$$\begin{aligned} T_{ij} &= C^{E}_{ijkl}\, S_{kl} - e_{kij} E_k \\ D_i &= e_{ikl}\, S_{kl} + \varepsilon^{S}_{ik}\, E_k \end{aligned} \tag{8.3}$$

where $i, j, k, l = 1, 2, 3$.

Terms T_{ij}, S_{kl}, D_i, and E_k are, respectively, components of the mechanical stress tensor (Newton per square meter), components of the mechanical strain tensor, components of the electric flux density (coulomb per square meter), and components of the electric field vector (volts per meter). The term C^{E}_{ijkl} represents the components of the elastic stiffness constant tensor, which are evaluated at constant electric field (in newton per square meter). Terms e_{ikl} and ε^{S}_{ik} are, respectively, components of the piezoelectric constant tensor (in coulomb per square meter), and components of the dielectric constant tensor evaluated at constant strain (in fermi per meter).

The components of the strain tensor S_{kl} are defined by

$$S_{kl} = \frac{1}{2}(u_{k,l} + u_{l,k}) \tag{8.4}$$

where u_l is the component no. l of the displacement vector (meters), and where $u_{k,l} = \partial u_k / \partial x_l$.

The electric and magnetic fields inside of a medium are described by Maxwell's equations, which relate the fields to the microscopic average properties of the material. When the quasistatic approximation is introduced [14], the electric field is derivable from a scalar electric potential:

$$E_i = -\phi_{,i} \tag{8.5}$$

where ϕ_i is the electric potential (volts). The following Maxwell's equation is also needed for describing a piezoelectric medium:

$$D_{i,i} = 0 \tag{8.6}$$

Finally, the equation of motion for a piezoelectric medium, not subjected to body forces, may be written:

$$T_{ij,j} = \rho \ddot{u}_i \tag{8.7}$$

where ρ represents the density of the material (in kilograms per cubic meter), being $\ddot{u}_l = \partial^2 u_l / \partial t^2$, and t the time (in seconds). The mechanical stress tensor T_{ij} is symmetric [13].

However, Eq. (8.3) can be expressed as a tensorial equation, which is a more compact expression for constitutive equations of piezoelectric materials. Thus, the

constitutive piezoelectric model is formulated as [14]

$$\begin{aligned}\mathbf{T} &= \mathbf{c}^E\mathbf{S} - \mathbf{e}^T\mathbf{E}\\ \mathbf{D} &= \mathbf{e}\mathbf{S} + \boldsymbol{\varepsilon}^S\mathbf{E}\end{aligned} \tag{8.8}$$

where $\mathbf{c}^E$ is the fourth-order elastic tensor, where the components are evaluated by constant electrical field. The term $\boldsymbol{\varepsilon}^S$ is the second-order tensor of dielectric constants, whose components are calculated by constant strain. The third-order tensor of piezoelectric coefficients is expressed by the term $\mathbf{e}$. Finally, terms $\mathbf{T}$ and $\mathbf{D}$ are the second-order stress tensor and the electric displacement vector, respectively. The symbol T indicates transpose.

8.3 Functionally Graded Piezoelectric Materials

8.3.1 Functionally Graded Materials (FGMs)

FGMs are composite materials whose properties vary gradually and continuously along a specific direction within the domain of the material. The property variation is generally achieved through the continuous change of the material microstructure [1] (Figure 8.1); in other words, FGMs are characterized by spatially varying microstructures created by nonuniform distributions of the constituent phases. This variation can be accomplish by using reinforcements with different properties, sizes, and shapes, as well as by interchanging the role of reinforcement and matrix (base) material in a continuous manner. In this last case, the volume fraction of

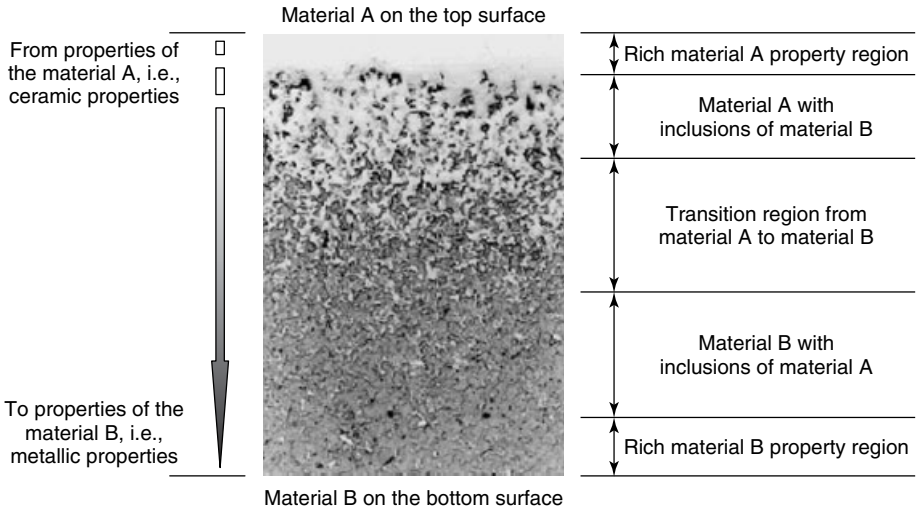

Figure 8.1 Microstructure of an FGM that is graded from material A to material B [15].

material phases continuously varies from 0 to 100% between two points of the structure; for instance, the material A of Figure 8.1 is gradually replaced by material B, smoothly varying through a transition zone [15, 16].

The main advantage of FGMs is their characteristic of ''combining'' advantage of desirable features of their constituent phases. For example, if a metal and a ceramic are used as a material base, FGMs could take advantage of heat and corrosion resistance typical of ceramics, and mechanical strength and toughness typical of metals; accordingly, a part of Figure 8.1 can represent a thermal barrier on the top surface (material A), by tacking advantage of the thermal properties of ceramics (low thermal conductivity and high melting point), while another part represents a material with high tensile strength and high resilience (metallic material B), on the bottom side [17], without any material interface. The absence of interfaces produces other interesting features such as reduction of thermal and mechanical stress concentration [18] and increased bonding strength and fatigue-lifetime [19].

The concept of FGMs is bioinspired (biomimic), as these materials occur in nature; for instance, in bones and teeth of animals [20–22], and trees such as the bamboo [23]. A dental crown is an excellent example of the FGM concept in natural structures: teeth require high resistance to friction and impact on the external area (enamel), and a flexible internal structure for reasons of fatigue and toughness [21, 22]. Other interesting example is the bamboo. Bamboo stalks are optimized composite materials that naturally exploit the concept of FGMs, as shown in Figure 8.2. The bamboo culm is an approximately cylindrical shell that is divided periodically by transversal diaphragms at nodes. Between 20 and 30% of the cross-sectional area of the culm is made of longitudinal fibers that are nonuniformly distributed through the wall thickness, the concentration being most dense near the exterior (Figure 8.2). The orientation of these fibers makes bamboo an orthotropic material with high strength along to fibers and low strength along its transverse direction [23].

In engineering applications, the FGM concept was originally proposed around 1984–1985 [17], when Japanese scientists researched advanced materials for aerospace industry; specifically, materials that bear the temperature gradient generated when a spacecraft returns to earth. In this case, the temperature gradient is approximately 1000 °C from the outside to the inside of the aircraft. They designed an FGM structure with ceramic properties on the outer surface, exposed to high temperature, and with properties of a thermally conductive material on the inner

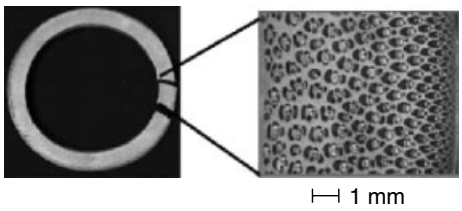

Figure 8.2 Cross section of bamboo culm showing radial nonuniform distribution of fibers through the thickness [23].

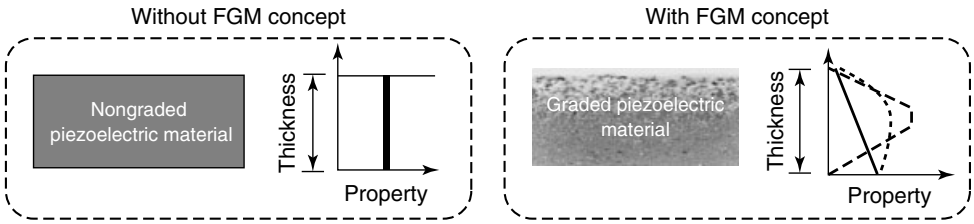

Figure 8.3 Sketch of a graded piezoelectric material: (a) nongraded piezoelectric material and (b) graded piezoelectric material based on FGM concept and considering several laws of gradation.

surface. Since then, the development of manufacture methods, design, and modeling techniques of FGMs has been the focus of several research groups worldwide. These researches focus mainly on thermal applications [18, 24]; bioengineering [20–22, 25]; industrial applications such as the design of watches, baseball cleats, razor blades, among others;[1)] and since the late 1990s, the design and fabrication of piezoelectric structures [4–8, 19, 26–30].

8.3.2 FGM Concept Applied to Piezoelectric Materials

As previously mentioned, piezoelectric materials have the property to convert electrical energy into mechanical energy and vice versa. Their main applications are in sensors and electromechanical actuators, as resonators in electronic equipment, and acoustic applications, as ultrasound transducers, naval hydrophones, and sonars. A recent trend has been the design and manufacture of piezoelectric transducers based on the FGM concept [19, 26–29]; in this case, the conventional single piezoelectric material is replaced by a graded piezoelectric material (Figures 8.3–8.5) and, consequently, some or all properties (elastic, piezoelectric, and/or dielectric properties) may change along one specific direction in which several functions or laws of gradation can be used (Figure 8.3).

Several authors have highlighted the advantages of the FGM concept when applied to piezoelectric structures [4–8, 19, 26, 28, 30]. In static or dynamic applications, the main advantages are reduction of the mechanical stress [26, 31], improved stress redistribution [26], maximization of output displacement, and increased bonding strength (and fatigue-life). For exemplifying the FGM concept when applied to piezoelectric structures, the case of a bimorph actuator can be considered. This kind of actuators is traditionally composed of two piezoelectric materials with opposite direction of polarization, and both are mechanically coupled by a metallic phase (electrode) (Figure 8.4). By applying an electric field along the thickness, the transducer will bend due to the fact the piezoelectric material will deform

1) More details are available in http://fgmdb.kakuda.jaxa.jp/others/e_product.html.

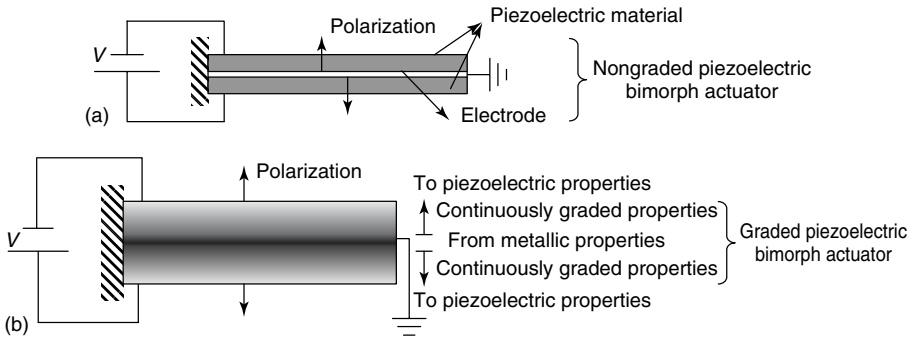

Figure 8.4 FGM concept applying to bimorph transducers: (a) nongraded piezoelectric transducer and (b) graded transducer from electrode (metallic) properties in the middle to piezoelectric properties on the top and bottom surfaces.

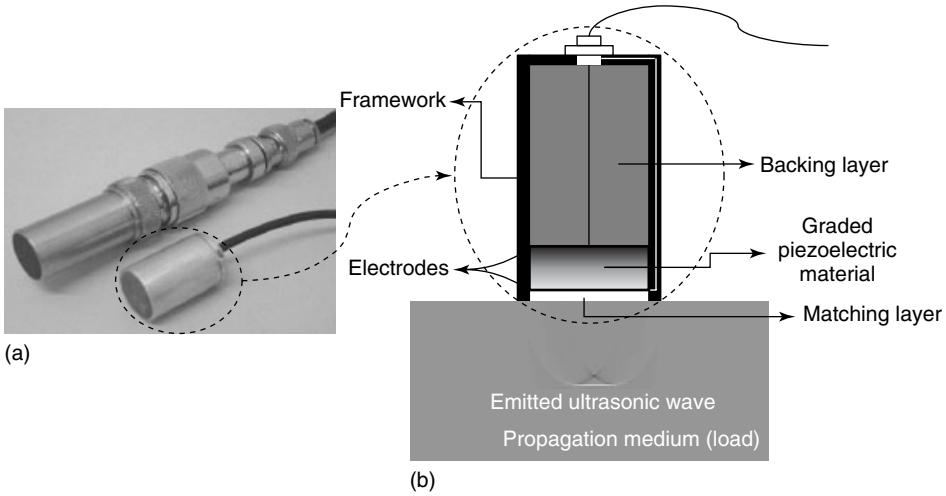

Figure 8.5 FGM concept applied to piezoelectric ultrasonic transducers: (a) photograph of a typical assembly of an ultrasonic transducer and (b) sketch of the same transducer considering a graded piezoelectric material.

in opposite directions. In dynamic applications, a critical issue in these bimorph actuators is the fatigue phenomena, which depends on the stress distribution into the actuator. It is clear that the stress distribution is not uniform due to the presence of material interfaces; specifically, between electrode/piezoelectric-material. The material interface will cause mechanical stress concentration, reduction of the fatigue limit, and accordingly, reduction of the transducer lifetime. However, by applying the FGM concept to a bimorph actuator, the material interface can be reduced or eliminated, as electrode properties can be smoothly varied from center to piezoelectric properties on the top and bottom surfaces (Figure 8.4).

In relation to durability, Qiu *et al.* [19] study the durability of graded piezoelectric bimorph actuators considering durability at low frequency (quasistatic operation) and durability at resonant frequency. In the former case, the graded and nongraded piezoelectric actuators are excited by 500 and 160 V (peak to peak), respectively. In a durability test, at 20 Hz (much lower than the resonance frequency of the first mode), the results show that the graded piezoelectric actuator did not break down after 300 h (2.16×10^7 cycles) of actuation, while the nongraded bimorph break down due to a crack after 138 h (about 10^7 cycles). In the second case (durability test at first resonance frequency), the graded and nongraded piezoelectric actuators are excited to 40 and 28 V (peak to peak), respectively. The average lifetime of a nongraded bimorph actuator is 24 min, and considering the FGM concept, graded actuators fail in the test period of 240 min.

In other application of piezoelectric materials, the FGM concept allows reducing reflection waves inside piezoelectric ultrasonic transducers [5] and obtaining acoustic responses with smaller time waveform (larger bandwidth) [4, 7, 8, 30] than nongraded piezoelectric transducers. These advantages are desirable for improving the axial resolution in medical imaging and nondestructive testing applications [32]. Particularly, considering that the piezoelectric material of an ultrasonic transducer is graded from a nonpiezoelectric to a piezoelectric material (or from piezoelectric property $e_{33} = 0$ on the top electrode to $e_{33} \neq 0$ on the bottom electrode), as shown in Figure 8.5, the larger bandwidth of the graded piezoelectric transducer is produced because the acoustic pulse is generated mainly from the surface with higher piezoelectric properties. In other words, as explained by Yamada *et al.* [4], the induced piezoelectric stress $T_3 = -e_{33}\ E_3$ is higher on the surface with $e_{33} \neq 0$ than on the surface with $e_{33} = 0$. Hence, the volumetric force $F_v = \partial T_3/\partial z$ (or spatial derivative of the induced piezoelectric stress), which is responsible for the generation of acoustic waves, is equal to zero on the surface without piezoelectric properties, and it has its maximum value on the opposite surface [4]. Accordingly, a single ultrasonic pulse is generated by an impulse excitation.

In addition, in piezoelectric ultrasonic transducers, the FGM concept could be used to reduce the material interfaces between piezoelectric-material/backing and piezoelectric-material/matching[2)] (Figure 8.5).

2) Generally, ultrasound transducers are composed of an active element (piezoelectric material) bonded to two passive and non-piezoelectric elements (backing and matching layers); thus, when the piezoelectric material is electrically excited, the transducer produces an ultrasonic wave in a specific medium (load), as shown in Figure 8.5. The backing layer damps the back wave, and the matching layer matches the piezoelectric material and load acoustic impedances. The active element of most acoustic transducers used today is a piezoelectric ceramic.

8.4
Finite Element Method for Piezoelectric Structures

8.4.1
The Variational Formulation for Piezoelectric Problems

The dynamic equations of a piezoelectric continuum can be derived from the Hamilton principle, in which the Lagrangian and the virtual work are properly adapted to include the electrical contributions as well as the mechanical ones. According to this principle, the displacements and electrical potentials are those that satisfy the following equation [33]:

$$\delta \int_{t_1}^{t_2} L \, \mathrm{d}t + \int_{t_1}^{t_2} \delta W \, \mathrm{d}t = 0 \tag{8.9}$$

where L is the Lagrangian term, W is the external work done by mechanical and electrical forces, and the term δ represents the variational. The Lagrangian is given by Tiersten [33]:

$$L = \int_{\Omega} \left(\frac{1}{2} \rho \, \dot{\mathbf{u}}^T \dot{\mathbf{u}} - H \right) \mathrm{d}\Omega \tag{8.10}$$

where the terms H and $\mathbf{u}$ are the electrical enthalpy and the displacement vector, respectively. The integration of Eq. (8.10) is performed over a piezoelectric body of volume Ω. Considering that the surface S of the body Ω is subjected to prescribed surface tractions ($\mathbf{F}$) and surface charge per unit area (Q), the virtual work δW is given by the following expression [33]:

$$\delta W = \int_{S} \left(\delta \mathbf{u}^T \mathbf{F} - \delta \varphi \; Q \right) \mathrm{d}S \tag{8.11}$$

where φ is the electrical potential. On the other hand, the enthalpy is expressed as

$$H = P - \mathbf{E}^T \mathbf{D} \tag{8.12}$$

with $\mathbf{E}$ being the electrical field vector, $\mathbf{D}$ the electrical displacement vector, and P the potential energy, which is given as

$$P = \frac{1}{2} \mathbf{S}^T \mathbf{T} + \frac{1}{2} \mathbf{E}^T \mathbf{D} \tag{8.13}$$

where $\mathbf{S}$ and $\mathbf{T}$ are the second-order strain and stress tensors, respectively. By replacing Eqs (8.13) in (8.12), and using this result in Eq. (8.10), we obtain

$$L = \int_{\Omega} \left(\frac{1}{2} \rho \, \dot{\mathbf{u}}^T \dot{\mathbf{u}} - \frac{1}{2} \mathbf{S}^T \mathbf{T} + \frac{1}{2} \mathbf{E}^T \mathbf{D} \right) \mathrm{d}\Omega \tag{8.14}$$

On the other hand, by substituting in Eq. (8.14) the constitutive equations of a piezoelectric material, which are expressed in Eq. (8.8), the Lagrangian is expressed as

$$L = \int_{\Omega} \frac{1}{2} \left(\rho \, \dot{\mathbf{u}}^T \dot{\mathbf{u}} - \mathbf{S}^T \mathbf{c}^E \mathbf{S} + \mathbf{S}^T \mathbf{e}^T \mathbf{E} + \mathbf{E}^T \mathbf{e} \, \mathbf{S} + \mathbf{E}^T \boldsymbol{\varepsilon}^S \mathbf{E} \right) \mathrm{d}\Omega \tag{8.15}$$

and by replacing both Eqs (8.11) and (8.15) in Hamilton's formula (8.9), we deduce

$$\int_{t_1}^{t_2} \left(\int_{\Omega} (\rho\, \delta\dot{\mathbf{u}}^T \dot{\mathbf{u}} - \delta\mathbf{S}^T \mathbf{c}^E \mathbf{S} + \delta\mathbf{S}^T \mathbf{e}^T \mathbf{E} + \delta\mathbf{E}^T \mathbf{e}\, \mathbf{S} + \delta\mathbf{E}^T \boldsymbol{\varepsilon}^S \mathbf{E})\, \mathrm{d}\Omega + \int_S (\delta\mathbf{u}^T \mathbf{F} - \delta\varphi\, Q)\, \mathrm{d}S \right) \mathrm{d}t = 0 \tag{8.16}$$

To complete the variational formulation for a piezoelectric medium, the first term of Eq. (8.16) is integrated by parts with relation to time:

$$\int_{t_1}^{t_2} \rho\delta\dot{\mathbf{u}}^T \dot{\mathbf{u}}\, \mathrm{d}t = \rho\delta\mathbf{u}^T \dot{\mathbf{u}}\Big|_{t_1}^{t_2} - \int_{t_1}^{t_2} \rho\delta\mathbf{u}^T \ddot{\mathbf{u}}\, \mathrm{d}t = -\int_{t_1}^{t_2} \rho\delta\mathbf{u}^T \ddot{\mathbf{u}}\, \mathrm{d}t \tag{8.17}$$

and by substituting Eq. (8.17) in Eq. (8.16), the final expression of the variational piezoelectric problem is found:

$$\int_{\Omega} (-\rho\, \delta\mathbf{u}^T \ddot{\mathbf{u}} - \delta\mathbf{S}^T \mathbf{c}^E \mathbf{S} + \delta\mathbf{S}^T \mathbf{e}^T \mathbf{E} + \delta\mathbf{E}^T \mathbf{e}\, \mathbf{S} + \delta\mathbf{E}^T \boldsymbol{\varepsilon}^S \mathbf{E})\, \mathrm{d}\Omega + \int_S (\delta\mathbf{u}^T \mathbf{F} - \delta\varphi\, Q)\, \mathrm{d}S = 0 \tag{8.18}$$

8.4.2 The Finite Element Formulation for Piezoelectric Problems

The FEM is an approximation technique for finding the solution of complex constitutive relations, as expressed in Section 8.1. The method consists of dividing the continuum domain Ω, into subdomains V^e, named *finite elements*. These elements are interconnected at a finite number of points, or nodes, where unknowns are defined. In piezoelectric domains, unknowns usually are displacements and electrical potentials. Within each finite element, unknowns are uniquely defined by the values they assume at the element nodes, by using interpolation functions, usually named *shape functions* [34].

For piezoelectric problems, the FEM considers that the displacement field $\mathbf{u}$ and electrical potential φ for each finite element e, are, respectively, approximated by nodal displacements $\mathbf{u}_e$, nodal electrical potentials $\boldsymbol{\varphi}_e$, and shape functions; thus [34]

$$\mathbf{u}^e = \mathbf{N}_\mathbf{u} \mathbf{u}_e \;\text{ and }\; \varphi^e = \mathbf{N}_\varphi \boldsymbol{\varphi}_e \tag{8.19}$$

where $\mathbf{N}_\mathbf{u}$ and $\mathbf{N}_\varphi$ are shape functions for mechanical and electrical problems, respectively. By deriving Eq. (8.19), the strain tensor $\mathbf{S}$ and electric field $\mathbf{E}$ can be written in the following form:

$$\mathbf{S}^e = \mathbf{B}_\mathbf{u} \mathbf{u}_e \;\text{ and }\; \mathbf{E}^e = -\mathbf{B}_\varphi\, \boldsymbol{\varphi}_e \tag{8.20}$$

where $\mathbf{B_u}$ and $\mathbf{B}_\varphi$ are the strain-displacement and voltage-gradient matrices, respectively, which can be expressed as

$$\mathbf{B_u} = \begin{bmatrix} \frac{\partial}{\partial x} & 0 & 0 & 0 & \frac{\partial}{\partial z} & \frac{\partial}{\partial y} \\ 0 & \frac{\partial}{\partial y} & 0 & \frac{\partial}{\partial z} & 0 & \frac{\partial}{\partial x} \\ 0 & 0 & \frac{\partial}{\partial z} & \frac{\partial}{\partial y} & \frac{\partial}{\partial x} & 0 \end{bmatrix}^T \mathbf{N_u} \quad \text{and} \quad \mathbf{B_u} = \begin{Bmatrix} \frac{\partial}{\partial x} \\ \frac{\partial}{\partial y} \\ \frac{\partial}{\partial z} \end{Bmatrix} \mathbf{N_u} \tag{8.21}$$

The terms x, y, and z are the Cartesian coordinates. By substituting Eqs (8.19) and (8.20) in Eq. (8.18), the variational piezoelectric problem becomes (where subscript e indicates finite element) for each finite element domain:

$$\begin{aligned} &\left(\delta \mathbf{u}^e\right)^T \left\{ -\left(\int_{V^e} \rho \mathbf{N}_\mathbf{u}^T \mathbf{N_u} \, \mathrm{d}V^e \right) \ddot{\mathbf{u}}^e - \left(\int_{V^e} \mathbf{B}_\mathbf{u}^T \mathbf{c}^E \mathbf{B_u} \, \mathrm{d}V^e \right) \mathbf{u}^e - \left(\int_{V^e} \mathbf{B}_\mathbf{u}^T \mathbf{e}^T \mathbf{B}_\varphi \, \mathrm{d}V^e \right) \varphi^e \right. \\ &\qquad \left. + \int_{S^e} \mathbf{N}_\mathbf{u}^T \mathbf{F} \, \mathrm{d}S^e \right\} + \ldots \\ &\left(\delta \boldsymbol{\varphi}^e\right)^T \left\{ -\left(\int_{V^e} \mathbf{B}_\varphi^T \mathbf{e} \mathbf{B_u} \, \mathrm{d}V^e \right) \mathbf{u}^e + \left(\int_{V^e} \mathbf{B}_\varphi^T \boldsymbol{\epsilon}^S \mathbf{B}_\varphi \, \mathrm{d}V^e \right) \boldsymbol{\varphi}^e - \int_{S^e} \mathbf{N}_\varphi^T Q \, \mathrm{d}S^e \right\} = 0 \end{aligned} \tag{8.22}$$

By grouping the terms that multiply $\delta \mathbf{u}_e^T$ and $\delta \boldsymbol{\varphi}_e^T$ in Eq. (8.22), two sets of matrix equations are obtained, yielding for each finite element, the following piezoelectric finite element formulation:

$$\begin{bmatrix} \mathbf{M}_{\mathbf{uu}}^e & 0 \\ 0 & 0 \end{bmatrix} \begin{Bmatrix} \ddot{\mathbf{u}}^e \\ \ddot{\boldsymbol{\varphi}}^e \end{Bmatrix} + \begin{bmatrix} \mathbf{K}_{\mathbf{uu}}^e & \mathbf{K}_{\mathbf{u}\varphi}^e \\ \mathbf{K}_{\mathbf{u}\varphi}^e & -\mathbf{K}_{\varphi\varphi}^e \end{bmatrix} \begin{Bmatrix} \mathbf{u}^e \\ \boldsymbol{\varphi}^e \end{Bmatrix} = \begin{Bmatrix} \mathbf{F}_p^e \\ \mathbf{Q}_p^e \end{Bmatrix} \tag{8.23}$$

where

$$\begin{aligned} \mathbf{M}_{\mathbf{uu}}^e &= \sum_{N_{\text{ele}}} \iiint \mathbf{N}_\mathbf{u}^T \, \rho\left(x, y, z\right) \mathbf{N_u} \, \mathrm{d}x \, \mathrm{d}y \, \mathrm{d}z; \\ \mathbf{K}_{\mathbf{uu}}^e &= \sum_{N_{\text{ele}}} \iiint \mathbf{B}_\mathbf{u}^T \, \mathbf{c}^E\left(x, y, z\right) \mathbf{B_u} \, \mathrm{d}x \, \mathrm{d}y \, \mathrm{d}z; \\ \mathbf{K}_{\mathbf{u}\varphi}^e &= \sum_{N_{\text{ele}}} \iiint \mathbf{B}_\mathbf{u}^T \, \mathbf{e}^T\left(x, y, z\right) \mathbf{B}_\varphi \, \mathrm{d}x \, \mathrm{d}y \, \mathrm{d}z; \\ \mathbf{K}_{\varphi\varphi}^e &= \sum_{N_{\text{ele}}} \iiint \mathbf{B}_\varphi^T \, \boldsymbol{\epsilon}^S\left(x, y, z\right) \mathbf{B}_\varphi \, \mathrm{d}x \, \mathrm{d}y \, \mathrm{d}z \end{aligned} \tag{8.24}$$

$$\mathbf{F}_\mathbf{p}^e = \int_S \mathbf{N}_\mathbf{u}^T \mathbf{F} \, \mathrm{d}S^e \quad \mathbf{Q}_\mathrm{p}^e = -\int_S \mathbf{N}_\varphi^T \mathbf{Q} \, dS^e \tag{8.25}$$

The terms $\mathbf{M}_{\mathbf{uu}}^e$, $\mathbf{K}_{\mathbf{uu}}^e$, $\mathbf{K}_{\mathbf{u}\varphi}^e$, and $\mathbf{K}_{\varphi\varphi}^e$ are, respectively, the mass, elastic, piezoelectric, and dielectric matrices; the terms x, y, and z explicitly represent the dependency of material properties with position, in graded piezoelectric systems.

According to FEM theory, matrices and vectors in Eq. (8.23) must be rearranged for the whole domain Ω by a process called *assembly*. Thus, global matrices and vectors of piezoelectric constitutive equations result from assembling the vectors and matrices of single elements [34]. In Eq. (8.24), assembly is represented by the summation symbol, and the term N_{ele} represents the total number of finite elements.

In addition, the matrix equation (8.23) may be adapted for a variety of different analyses, such as static, modal, harmonic, transient types [34], which are given (the global piezoelectric system is considered):

- **Static analysis**:

$$\begin{bmatrix} \mathbf{K_{uu}} & \mathbf{K_{u\varphi}} \\ \mathbf{K_{u\varphi}^T} & -\mathbf{K_{\varphi\varphi}} \end{bmatrix} \begin{Bmatrix} \mathbf{u} \\ \boldsymbol{\varphi} \end{Bmatrix} = \begin{Bmatrix} \mathbf{F}_p \\ \mathbf{Q}_p \end{Bmatrix} \tag{8.26}$$

- **Modal analysis**:

$$\begin{aligned} &-\lambda \begin{bmatrix} \mathbf{M_{uu}} & 0 \\ 0 & 0 \end{bmatrix} \begin{Bmatrix} \boldsymbol{\Psi}_\mathbf{u} \\ \boldsymbol{\Psi}_\varphi \end{Bmatrix} \\ &+ \begin{bmatrix} \mathbf{K_{uu}} & \mathbf{K_{u\varphi}} \\ \mathbf{K_{u\varphi}^T} & -\mathbf{K_{\varphi\varphi}} \end{bmatrix} \begin{Bmatrix} \boldsymbol{\Psi}_\mathbf{u} \\ \boldsymbol{\Psi}_\varphi \end{Bmatrix} = \begin{Bmatrix} 0 \\ 0 \end{Bmatrix} \text{ with } \lambda = \omega^2 \end{aligned} \tag{8.27}$$

- **Harmonic analysis**:

$$\left(-\Omega_c^2 \begin{bmatrix} \mathbf{M_{uu}} & 0 \\ 0 & 0 \end{bmatrix} + \begin{bmatrix} \mathbf{K_{uu}} & \mathbf{K_{u\varphi}} \\ \mathbf{K_{u\varphi}^T} & -\mathbf{K_{\varphi\varphi}} \end{bmatrix} \right) \begin{Bmatrix} \mathbf{u}_0 \\ \boldsymbol{\varphi}_0 \end{Bmatrix} = \begin{Bmatrix} \mathbf{F}_0 \\ \mathbf{Q}_0 \end{Bmatrix} \tag{8.28}$$

- **Transient analysis**:

$$\begin{aligned} &\begin{bmatrix} \mathbf{M_{uu}} & 0 \\ 0 & 0 \end{bmatrix} \begin{Bmatrix} \ddot{\mathbf{u}} \\ \ddot{\boldsymbol{\varphi}} \end{Bmatrix} + \frac{1}{\omega_0} \begin{bmatrix} \mathbf{K'_{uu}} & \mathbf{K'_{u\varphi}} \\ \mathbf{K'^T_{u\varphi}} & -\mathbf{K'_{\varphi\varphi}} \end{bmatrix} \begin{Bmatrix} \dot{\mathbf{u}} \\ \dot{\boldsymbol{\varphi}} \end{Bmatrix} \\ &+ \begin{bmatrix} \mathbf{K_{uu}} & \mathbf{K_{u\varphi}} \\ \mathbf{K_{u\varphi}^T} & -\mathbf{K_{\varphi\varphi}} \end{bmatrix} \begin{Bmatrix} \mathbf{u} \\ \boldsymbol{\varphi} \end{Bmatrix} = \begin{Bmatrix} \mathbf{F}_p \\ \mathbf{Q}_p \end{Bmatrix} \end{aligned} \tag{8.29}$$

where λ and ω represent eigenvalue and natural frequency, respectively. The term $\boldsymbol{\psi}$ represents eigenvectors, and the term Ω_c is the circular frequency of a harmonic input excitation. Each of these analysis cases requires specific conditioning and computation techniques. A full description of theses techniques is a topic that is beyond the scope of this chapter.

8.4.3 Modeling Graded Piezoelectric Structures by Using the FEM

When graded piezoelectric structures are simulated, properties must change continuously inside piezoelectric domain, which means that matrices of Eq. (8.23) must be described by a continuous function that depends on Cartesian position (x, y, z). In literature, there are several material models applied to estimate the

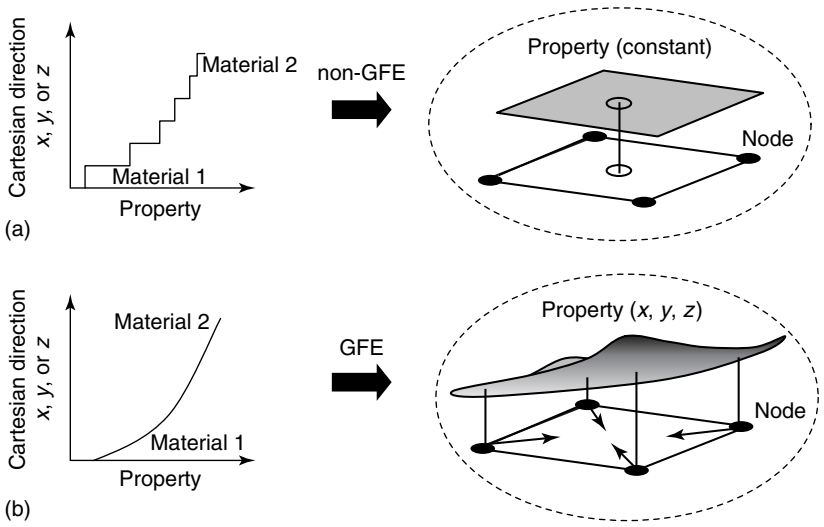

Figure 8.6 Finite element modeling of FGMs: (a) homogeneous finite element and (b) graded finite element.

effective properties of composite materials, which could be used in FGM, such as the Mori–Tanaka and the self-consistent models [35]. Other works treat the nonhomogeneity of the material, inherent in the problem, by using homogeneous finite elements with constant material properties at the element level; in this case, properties are evaluated at the centroid of each element (Figure 8.6a). This element-wise approach is close to the multilayer one, which depends on the number of layers utilized; accordingly, a layer convergence analysis must be performed in addition to finite element convergence, as shown in Ref. [30], for reducing the difference between the multilayer approach and the continuous material distribution. On the other hand, the multilayer approach leads to undesirable discontinuities of the stress [26] and strain fields [36] and discontinuous material gradation [30].

A more natural way of representing the material distribution in a graded material is based on graded finite elements (GFEs), which incorporate the material property gradient at the size scale of the element (Figure 8.6b) and reduce the discontinuity of the material distribution. Specifically, for static problems, Kim and Paulino [36] and Silva *et al.* [37] demonstrate that, by using the generalized isoparametric formulation (GIF), smoother and more accurate results are obtained in relation to element-wise approach. Essentially, the GIF leads to GFEs, where the material property gradient is continuously interpolated inside each finite element based on property values at each finite element node (Figure 8.6b). By employing the GIF, the same interpolation functions are used to interpolate displacements and electric potential, spatial coordinates (x, y, z), and material properties inside each finite element. Specifically, finite element shape functions N are used as interpolation functions.

For material properties, and by using the GIF, the density, ρ, and the elastic, C^E_{ijkl}, piezoelectric, e_{ikl}, and dielectric, ε^S_{ik}, material properties of a piezoelectric finite element can be written as

$$\rho(x,y,z) = \sum_{n=1}^{n_d} N_n(x,y,z)\ \rho_n, \quad C^E_{ijkl}(x,y,z) = \sum_{n=1}^{n_d} N_n(x,y,z)\ \left(C^E_{ijkl}\right)_n,$$
$$e_{ikl}(x,y,z) = \sum_{n=1}^{n_d} N_n(x,y,z)\ (e_{ikl})_n,$$
$$\varepsilon^S_{ik}(x,y,z) = \sum_{n=1}^{n_d} N_n(x,y,z)\left(\varepsilon^S_{ik}\right)_n \quad \text{for } i,j,k,l = 1,2,3 \tag{8.30}$$

where n_d is the number of nodes per finite element. When the GFE is implemented, the material properties must remain inside the integrals in Eq. (8.24), and they must be properly integrated. On the contrary, in homogeneous finite elements, these properties usually are constants.

8.5 Influence of Property Scale in Piezotransducer Performance

8.5.1 Graded Piezotransducers in Ultrasonic Applications

A very interesting application of piezoelectric materials is in ultrasonics. Piezoelectric ultrasonic transducers are mainly applied to nondestructive tests and medical images. In the last case, ultrasonic imaging has quickly replaced conventional X-rays in many clinical applications because of its image quality, safety, and low cost. Usually, a piezoelectric ultrasonic transducer is composed of a backing and matching layers and a piezoelectric disk, as shown in Figure 8.5. The piezoelectric disk is capable of transmitting and receiving pressure waves directed into a propagation medium such as the human body. Such transducers normally comprise single or multistacking element piezoelectric disks, which vibrate in response to an applied voltage for radiating a front-side wave in a specific medium (solid, liquid, or air), or produce an electrical potential when a pressure wave is received.

To obtain high-quality images, the ultrasonic transducer must be constructed so as to produce specified frequencies of pressure waves. Generally speaking, low-frequency pressure waves provide deep penetration into the medium (e.g., the human body); however, they produce poor-resolution images due to the length of the transmitted wavelengths. On the other hand, high-frequency pressure waves provide high resolution, however, with poor penetration. Accordingly, the selection of a transmitting frequency involves balancing resolution and penetration concerns. Unfortunately, there is a trade-off between resolution and deeper penetration. Traditionally, the frequency selection problem has been addressed by selecting the

highest imaging frequency that offers adequate penetration for a given application. For example, in adults' cardiac imaging, frequencies in the 2–3 MHz range are typically selected in order to penetrate the human chest wall [38].

Recently, a new method has been studied in an effort to obtain both high resolution and deep penetration: treating piezoelectric ultrasonic transducers as graded structures (based on FGM concept). Hence, by focusing on the piezoelectric material, the piezoelectric disk of Figure 8.5 is assumed as a graded piezoelectric disk [30].

For studying this kind of graded piezoelectric transducers, which are based on the acoustic transmission line theory, and referred to as *functionally graded piezoelectric ultrasonic transducer*s – FGPUTs here, a simple and nonexpensive computational cost approach is used [39]. According to acoustic transmission line theory, an FGPUT can be represented as a three-port system (Figure 8.7): one electric and two mechanical ports. The acoustic interaction of the graded piezoelectric disk with the propagating medium and the backing layer (both media are considered to be semi-infinite) is represented by mechanical ports. The electric port represents the electric interaction between the graded piezoelectric disk and the electric excitation circuit. This electrical circuit has a signal generator (E_g) and an internal resistance (R). Nevertheless, to complete the analytical model, an intermediate system must be assumed: the matching layer. The iteration between matching layer and graded piezoelectric disk is modeled as a system with two mechanical ports. In acoustic transmission line theory, the thickness of electrodes is supposed to be sufficiently small compared to acoustic wavelength involved, so

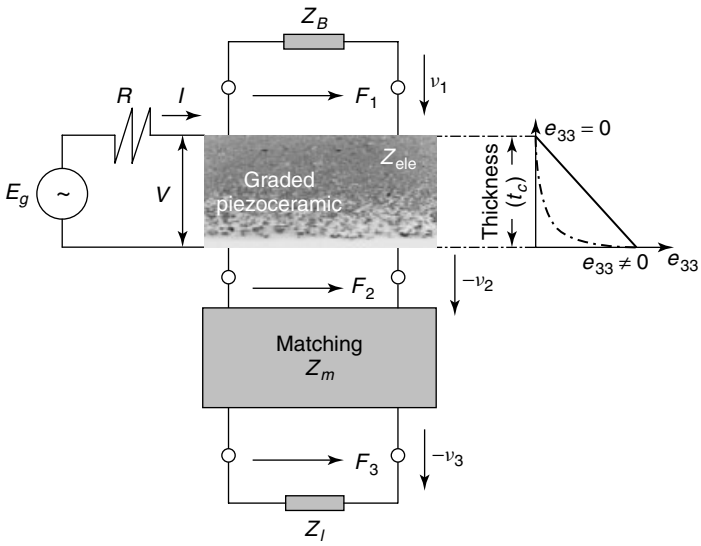

Figure 8.7 Sketch of an FGPUT, where Z_B, Z_{ele}, Z_m, and Z_l represent the electrical impedance of backing layer, graded piezoceramic, matching layer, and load, respectively.

the perturbation of the pressure distribution on load-medium, caused by these electrodes, can be neglected.

The goal of the FGPUT modeling, based on the acoustic transmission line theory, is to find a relationship between the electric current (I) and the electric potential (V) in the electric circuit with the force (F_3) and the particle velocity (v_3) radiated into the propagation media (Figure 8.7). This relationship is expressed in matrix form as [30]

$$\begin{pmatrix} V \\ I \end{pmatrix} = \begin{pmatrix} T_{11} & T_{12} \\ T_{21} & T_{22} \end{pmatrix} \begin{pmatrix} F_3 \\ v_3 \end{pmatrix} = [A][M] \begin{pmatrix} F_3 \\ v_3 \end{pmatrix} \tag{8.31}$$

where

$$\begin{pmatrix} V \\ I \end{pmatrix} = \begin{pmatrix} A_{11} & A_{12} \\ A_{21} & A_{22} \end{pmatrix} \begin{pmatrix} F_2 \\ v_2 \end{pmatrix} = [A] \begin{pmatrix} F_2 \\ v_2 \end{pmatrix}$$

$$\text{and} \quad \begin{pmatrix} F_2 \\ v_2 \end{pmatrix} = \begin{pmatrix} M_{11} & M_{12} \\ M_{21} & M_{22} \end{pmatrix} \begin{pmatrix} F_3 \\ v_3 \end{pmatrix} = [M] \begin{pmatrix} F_3 \\ v_3 \end{pmatrix} \tag{8.32}$$

Matrices **A** and **M**, in Eqs (8.32) and (8.33), essentially depend on gradation function assumed in the graded piezoelectric disk. Details of mathematical procedure for finding matrices **A** and **B** can be found in Ref. [30]. Two gradation functions are studied by Rubio *et al.* [30]: linear and exponential functions, where the gradation is considered along the thickness direction for the piezoelectric property e_{33} (Figure 8.7). In both cases, piezoelectric properties are graded from a nonpiezoelectric material, on the top surface, to a piezoelectric one, on the bottom surface (or from $e_{33} = 0$ to $e_{33} \neq 0$).

To complete the FGPUT modeling and based on Eqs (8.32) and (8.33), one can find the expressions, in the frequency domain, of the transmission transfer function (TTF) and the input electrical impedance of the graded piezoelectric disk (Z_{ele}). The TTF is a relationship between the mechanical force on load-medium (F_3) and the electric potential of the voltage generator (E_g), and Z_{ele} is a relationship between the electric current (I) and the electric potential (V) in the electric circuit. Hence, terms TTF and Z_{ele} can be written as follows:

$$\text{TTF} = \frac{F_3}{E_g} = \frac{Z_l}{T_{11}Z_l + T_{12} + R\,(T_{21}Z_l + T_{22})} \tag{8.33a}$$

$$Z_{ele} = \frac{V}{I} = \frac{A_{12}}{A_{22}} \tag{8.33b}$$

Overall, on the basis of the acoustic transmission line theory and considering FGPUTs, one can explore the FGM concept in medical imaging applications. Thus, it is assumed that an FGPUT, with a thickness of the piezoelectric disk equal to 1 mm, as shown in Figure 8.5, radiates a ultrasonic wave inside a water medium[3)] when the piezoelectric disk is excited with a half-sine electrical wave, whose fundamental frequency is $f_0 = 2.3$ MHz.

3) Water has acoustics impedance close to human tissue one [40].

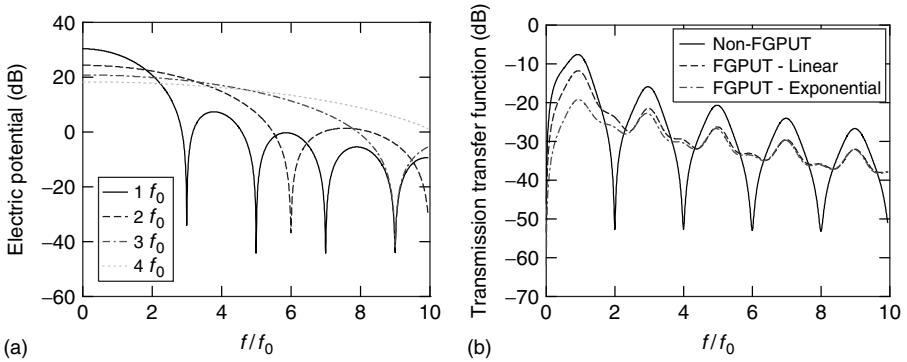

Figure 8.8 (a) Spectrum of several electrical input excitations (each with different fundamental frequency) and (b) normalized-frequency transmission transfer function (TTF) for both non-FGPUT and FGPUT with linear and exponential gradation functions [30].

Figure 8.8a shows the frequency spectra of an input signal at $f_0 = 2.3$ MHz; additionally, Figure 8.8a also shows frequency spectra of other input signals, however, with fundamental frequencies equal to $2f_0$, $3f_0$, and $4f_0$. From Figure 8.8a, it is clear that when the fundamental frequency is increased, its spectrum exhibits higher broadband; however, with less amplitude. On the other hand, Figure 8.8b presents the frequency spectra of the TTF, which is calculated by using Eq. (8.33a). For the non-FGPUT, it is observed that its frequency spectrum ''falls to zero'' in even-order modes ($f/f_0 = 2, 4, 6, \ldots$), while for the FGPUT (considering linear and exponential gradations), its frequency spectra do not fall to zero either for even or for odd order modes. For this reason, the bandwidth of an FGPUT is only limited by the bandwidth of the input excitation; on the other hand, the bandwidth of a non-FGPUT is limited by both input excitation and TTF bandwidths. However, the FGPUT represents a system with less gain in relation to non-FGPUT one. As a result, the FGPUT is a transducer with less output power (or less power delivered to fluid), because gradation functions depict an FGPUT with less ''regions'' of high piezoelectric properties than the non-FGPUT. On the other hand, the output signal (Figure 8.9), which is the dot product between TTF and input signal spectra, clearly highlights the incremented broadband, which is achieved by using the FGM concept, with both linear and exponential gradation functions.

The larger bandwidth of the FGPUT is produced because the acoustic pulse is generated mainly from the surface with high piezoelectric properties, while the opposite surface generates small vibration. In other words, as explained in Ref. [4], the induced piezoelectric stress $T_3 = -e_{33}E_3$ is higher on the surface with $e_{33} \neq 0$ than on the surface with $e_{33} = 0$. Thus, the volumetric force $F_v = \partial T_3/\partial z$ (spatial derivative of the induced stress), which is responsible for acoustic wave generation, is equal to zero on the surface without piezoelectric properties, and it has its maximum value on the opposite surface. For this reason, a single ultrasonic pulse is generated by an impulse excitation, which exhibits higher bandwidth.

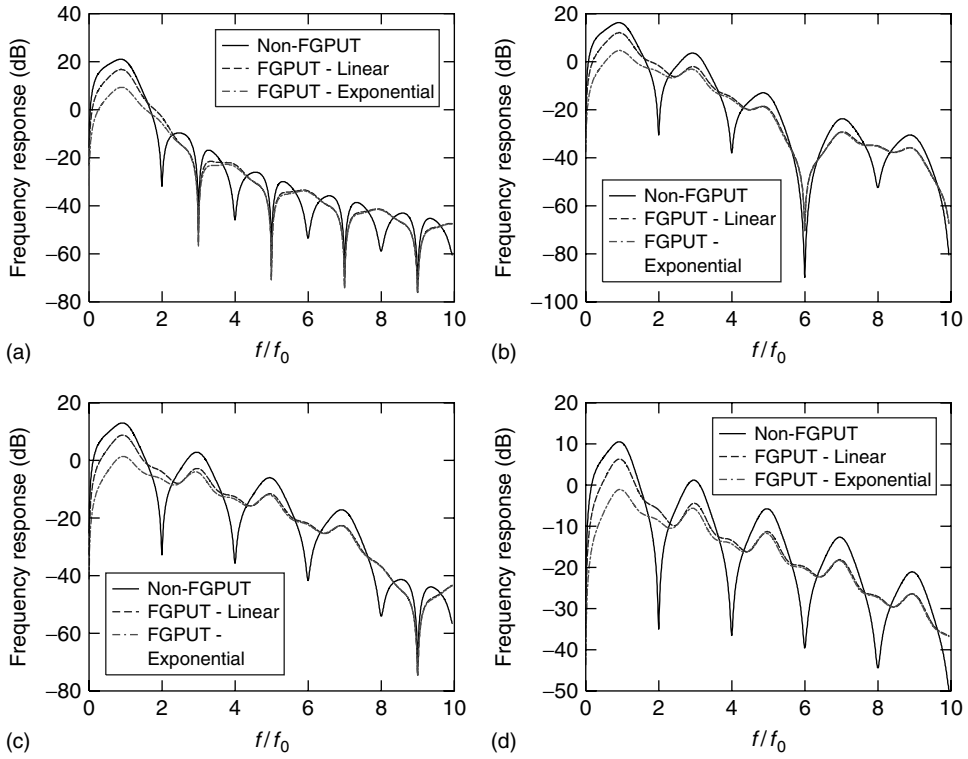

Figure 8.9 Spectrum of output signals for non-FGPUT and FGPUT systems considering several input excitations: (a) at $1f_0$; (b) at $2f_0$; (c) at $3f_0$; and (d) at $4f_0$.

Another interesting aspect is the analysis of the electrical impedance of an FGPUT with linear and exponential gradation functions, which can be computed by using Eq. (8.33b) [30]. Figure 8.10 shows normalized-frequency electrical impedance curves (focusing on thickness vibration modes), for both linear and exponential gradation functions of the piezoelectric property e_{33} (Figure 8.7). Specifically, Figure 8.10 shows the electrical impedance of only the graded piezoelectric disk; in other words, the FGPUT is simulated without backing and matching layers. It is observed that in FGPUT, electrical impedance curves appear with even and odd vibration modes; by contrast, in the non-FGPUT, curves appear with only odd vibration modes. This result indicates that it is possible to achieve, by using the FGM concept, more or less resonance modes in selective frequencies according to the gradation function used.

From Figures 8.8–8.10, it is observed that FGPUTs arise as a new and versatile alternative for applications in medical and nondestructive images. Specifically, in medical images, FGPUTs can obtain high resolution and deep penetration, when operated by using the harmonic imaging technique because they exhibit large bandwidth (Figures 8.8b and 8.9). Hence, it is possible to excite an object

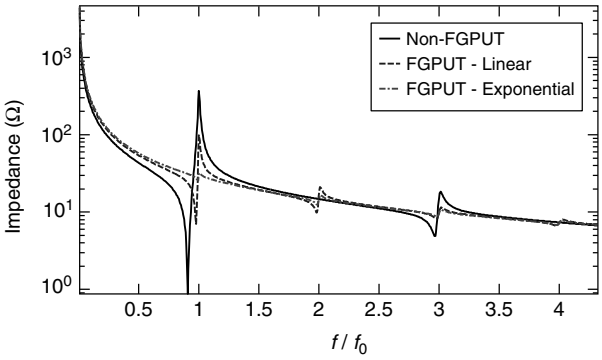

Figure 8.10 Electric impedance calculated by using Eq. (8.33b): for a non-FGPUT and an FGPUT considering linear and exponential gradations.

to be imaged, such as human tissues, by transmitting at a low (and therefore deeply penetrating) fundamental frequency (f_0) and receiving at a harmonic wave having a higher frequency (e.g., human tissues develop and return their own non-fundamental frequencies, for instance, $2f_0$), which can be used to form a high-resolution image of the object. In fact, in medical imagining application and by using FGPUTs, a wave having a frequency less than 2 MHz can be transmitted into the human body (e.g., human chest for cardiac imaging) and one or more harmonic waves having frequencies equal, and/or greater than 3 MHz can be received to form the image. By imaging in this manner (using FGPUTs in conjunction with the harmonic imaging technique), deep penetration can be achieved without a concomitant loss of image resolution.

8.5.2
Further Consideration of the Influence of Property Scale: Optimal Material Gradation Functions

As observed in the above section, the gradation function can influence the performance of graded piezoelectric transducers. This fact has been confirmed by several authors, for example, Almajid *et al.* [26], Taya *et al.* [28], and Rubio *et al.* [30]. This suggests using an optimization method for finding the optimal gradation function along a specific direction. Among the optimization methods, the topology optimization method (TOM) has shown to be a successfully technique for determining the best-property gradation function for a specific static or dynamic application [41–43].[4)]

For exemplifying the above idea, one can design an FGPUT, finding the optimal gradation function, in order to maximize a specific objective function. Thus, for

4) Details about topology optimization method can be found in the work by Bendsøe and Sigmund [44].

FGPUT design, the topology optimization problem can be formulated for finding the optimal gradation law that allows achieving multimodal or unimodal frequency response. These kinds of response define the type of generated acoustic wave, either short pulse (unimodal response) or continuous wave (multimodal response). Furthermore, the transducer is required to oscillate in a thickness extensional mode (pistonlike mode), aiming at acoustic wave generation applications.

For unimodal transducers, the electromechanical coupling of a desirable mode k must be maximized, and the electromechanical coupling of the adjacent modes (mode number $k + a_1$ with $a_1 = 1, 2, \ldots, A_1$, and/or $k - a_2$ with $a_2 = 1, 2, \ldots, A_2$) must be minimized. Additionally, the resonance frequencies of the modes $k_1 = k + a_1$ with $a_1 = 1, 2, \ldots, A_1$ must be maximized, and the resonance frequencies of the modes $k_2 = k - a_2$ with $a_2 = 1, 2, \ldots, A_2$ must be minimized. For multimodal transducers, electromechanical couplings of a mode set must be maximized, and their resonance frequencies must be approximated. Accordingly, for unimodal (F_1) and multimodal (F_2) transducers, the objective functions can be formulated as follows [45]:

$$\begin{aligned} F_1 = w_k\left(A_{r_k}\right) &- \left[\frac{1}{\alpha_1}\left(\sum_{k_1=1}^{A_1} w_{1k_1}\left(A_{r_{k_1}}\right)^{n_1}\right)\right]^{1/n_1} \\ &- \left[\frac{1}{\alpha_2}\left(\sum_{k_2=1}^{A_2} w_{2k_2}\left(A_{r_{k_2}}\right)^{n_2}\right)\right]^{1/n_2} + \left[\frac{1}{\alpha_3}\left(\sum_{k_1=1}^{A_1} w_{3_{k_1}}\left(\lambda_{r_{k_1}}\right)^{n_3}\right)\right]^{1/n_3} \\ &- \left[\frac{1}{\alpha_4}\left(\sum_{k_2=1}^{A_2} w_{4k_2}\left(\lambda_{r_{k_2}}\right)^{n_4}\right)\right]^{1/n_4} \end{aligned} \tag{8.34}$$

with

$$\alpha_1 = \sum_{k_1=1}^{A_1} w_{1k_1};\ \alpha_2 = \sum_{k_2=1}^{A_2} w_{2k_2};\ \alpha_3 = \sum_{k_1=1}^{A_1} w_{3k_1};$$

$$\alpha_4 = \sum_{k_2=1}^{A_2} w_{4k_2};\ n_m = -1, -3, -5, -7 \ldots;\ m = 1, 2, 3, 4$$

$$F_2 = \left[\frac{1}{\alpha_1}\left(\sum_{k=1}^{m} w_k\left(A_{r_k}\right)^{n_1}\right)\right]^{1/n_1} - \left[\frac{1}{\alpha_2}\sum_{k=1}^{m}\frac{1}{\lambda_{0_k}^2}\left(\lambda_{r_k}^2 - \lambda_{0_k}^2\right)\right]^{1/n_2} \tag{8.35}$$

with

$$\alpha_1 = \sum_{k=1}^{m} w_k; \quad \alpha_2 = \sum_{k=1}^{m}\frac{1}{\lambda_{0_k}^2}; \quad \lambda_{r_k} = \omega_{r_k}^2;$$

$$n_1 = -1, -3, -5, -7 \ldots; \quad n_2 = \pm 2, \pm 4, \pm 6, \pm 8 \ldots$$

where, for unimodal transducers (Eq. (8.34)), terms A_{r_k}, $A_{r_{k_1}}$, and $A_{r_{k_2}}$ represent the electromechanical coupling (measured by the piezoelectric modal constant – PMC [46]) of the desirable mode, and left and right adjacent modes, respectively. Terms

w_k, $w_{i_{k_1}}$ $(i = 1, 3)$, and $w_{j_{k_2}}$ $(j = 2, 4)$ are the weight coefficients for each mode considered in the objective function F_1. Finally, terms $\lambda_{r_{k_1}}$ and $\lambda_{r_{k_2}}$ represent eigenvalues of the left and the right modes with relation to the desirable one (mode number k), and the term n is a given power. For multimodal transducers (Eq. (8.35)), the constant m is the number of modes considered; the terms λ_{r_k} and λ_{0_k} are the current and desirable (or user-defined) eigenvalues for mode k $(k = 1, 2, \ldots, m)$, respectively; and ω_{r_k} are the resonance frequencies for mode k $(k = 1, 2, \ldots, m)$.

The optimization problem is formulated as finding the material gradation of FGPUT, which maximizes the multiobjective function F_1 or F_2 subjected to a piezoelectric volume constraint. This constraint is implemented to control the amount of piezoelectric material into the two-dimensional design domain, Ω. The optimization problem is expressed as

$$\begin{aligned} &\underset{\rho_{\mathrm{TOM}}(x,y)}{\text{maximize}} && F_i \; i = 1 \text{ or } 2 \\ &\text{subjected to} && \int_{\Omega} \rho_{\mathrm{TOM}}(x, y)\mathrm{d}\Omega - \Omega_s \leq 0\,; \\ &&& 0 \leq \rho_{\mathrm{TOM}}(x, y) \leq 1 \\ &&& \text{equilibrium and constitutive equations} \end{aligned} \tag{8.36}$$

where $\rho_{\mathrm{TOM}}(x, y)$ is the design variable (pseudodensity) at Cartesian coordinates x and y. The term Ω_s describes the amount of piezoelectric material in the two-dimensional domain Ω.

The last requirement (mode shape tracking) is achieved by using the modal assurance criterion (MAC) [47], which is used to compare eigenmodes and to track the desirable eigenvalue and/or eigenvector along the iterative process of the TOM. Besides, to treat the gradation in FGPUT, material properties are continuously interpolated inside each finite element based on property values at each finite element node, as explained in Section 8.4.3. On the other hand, the continuum approximation of material distribution (CAMD) concept [48] is used to continuously represent the pseudodensity distribution. The CAMD considers that design variables inside each finite element are interpolated by using, for instance, the finite element shape functions N. Thus, the pseudodensity ρ^e_{TOM} at each GFE e can be expressed as

$$\rho^e_{\mathrm{TOM}}(x, y) = \sum_{i=1}^{n_d} \rho^n_{\mathrm{TOM}_i} N_i(x, y) \tag{8.37}$$

where $\rho^n_{\mathrm{TOM}_i}$ and N_i are, respectively, the nodal design variable and shape function for node $i (i = 1, \ldots, n_d)$, and n_d is the number of nodes at each finite element. This formulation allows a continuous distribution of material along the design domain instead of the traditional piecewise material distribution.

Additionally, to achieve an explicit gradient control, a projection technique can be implemented as explained in Ref. [49].

To illustrate the design of an FGPUT based on TOM, one can consider the design domain shown in Figure 8.11, for designing a unimodal and a multimodal FGPUT considering plane strain assumption. The design domain is specified as a

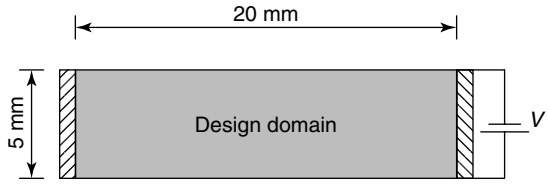

Figure 8.11 Design domain for FGPUT design.

20 mm × 5 mm rectangle with two fixed supports at the end of the left- and right-hand sides. The idea is to simultaneously distribute two types of materials into the design domain. The material *type 1* is represented by a PZT-5A piezoelectric ceramic and the material *type 2* is a PZT-5H. Initially, the design domain contains only PZT-5A material and a material gradation along thickness direction is assumed. In addition, a mesh of 50 × 30 finite elements is adopted.

Figure 8.12 shows the result when a unimodal FGPUTs is designed. It is observed that for the unimodal transducer, the optimal material gradation depicts an FGPUT with rich region of piezoelectric material PZT-5A in the middle and rich region of piezoelectric material PZT-5H on the top and bottom surfaces (Figure 8.12a).[5] The material gradation is found to allow the electromechanical coupling value (measured by the PMC [46]) of the pistonlike mode to increase by 59% while the PMC values of adjacent modes decrease approximately by 75% (Figure 8.12b).

The designed multimodal transducer is shown in Figure 8.13. The final material gradation represents an FGPUT with regions rich in piezoelectric properties PZT-5A around layers 10 and 23 and PZT-5H on the top and bottom surfaces. The optimal material gradation increases the PMC value of the pistonlike mode by 15%, while the PMC values of the left and right adjacent modes are increased by 15 and 181%, respectively. In both uni- and multimodal designs, the pistonlike mode is retained, which represents the mode with highest electromechanical coupling.

8.6 Influence of Microscale

The combination of a piezoelectric material (polymer or ceramic) with other materials (including air-filled voids) usually results in new composites, called *piezocomposites*, that offer substantial advantages over conventional piezoelectric

5) Observe that the optimization problem is treated as layerlike optimization problem; in other words, the design variables are assumed to be equal at each interface between finite elements. This approach allows manufacturing FGPUTs by sintering a layer-structured ceramic green body without using adhesive material.

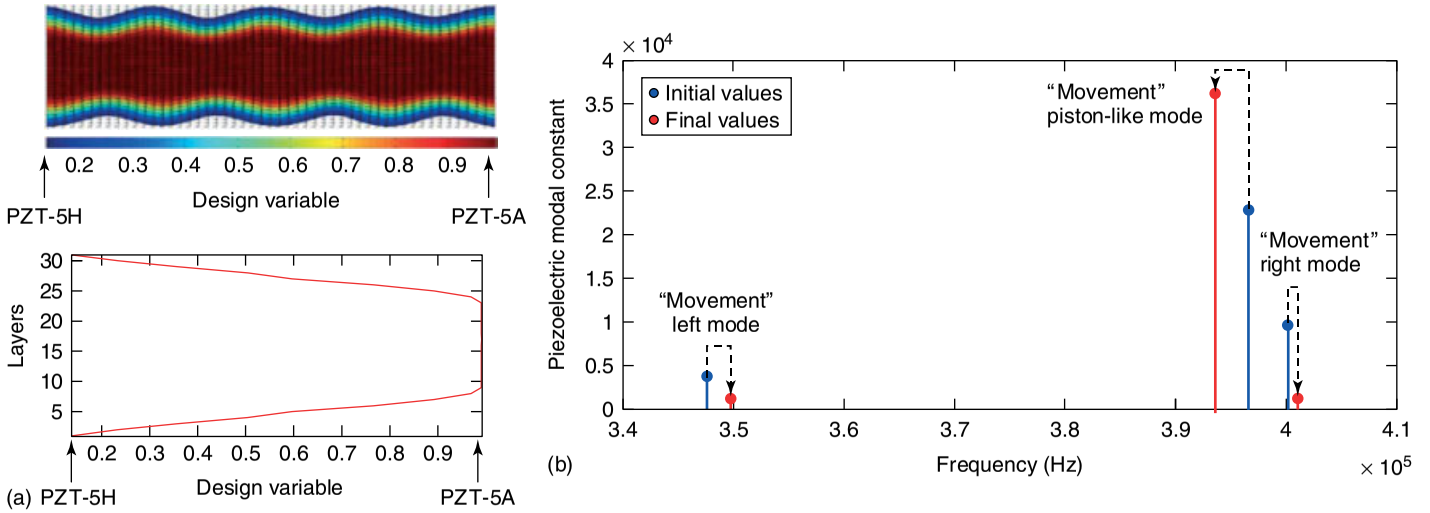

Figure 8.12 Design of a unimodal FGPUT: (a) pistonlike mode (dashed and solid lines, respectively, depict nondeformed and deformed structures) and final material distribution and (b) initial and final frequency response [45].

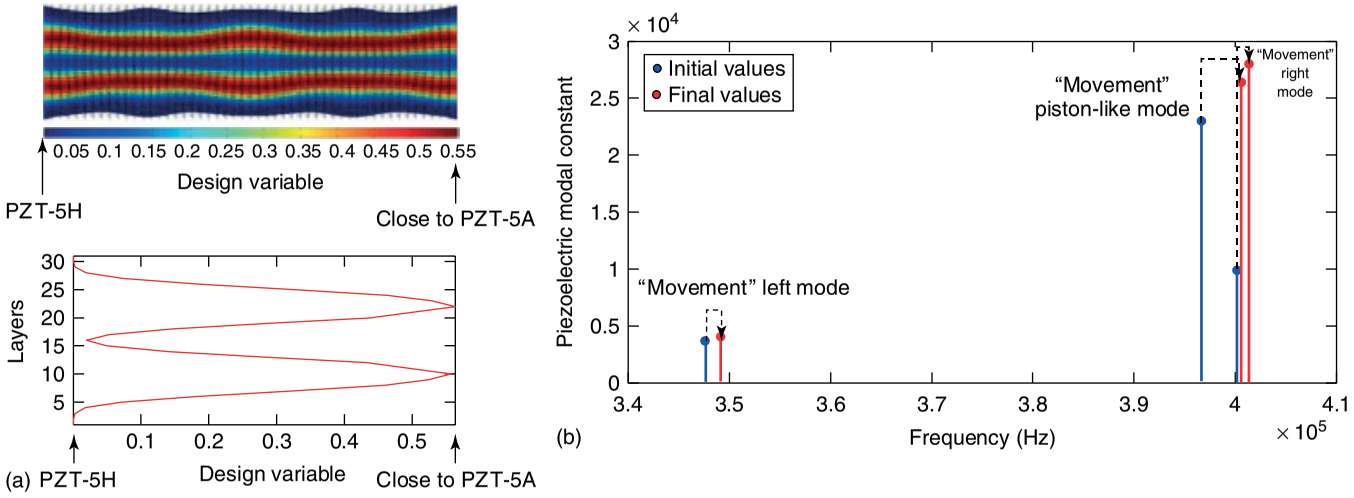

Figure 8.13 Design of a multimodal FGPUT: (a) pistonlike mode (dashed and solid lines, respectively, depict nondeformed and deformed structures) and final material distribution and (b) initial and final frequency response [45].

materials. The advantages are high electromechanical coupling, which measures energy conversion in the piezocomposite and therefore its sensitivity, and low acoustic impedance, which helps to transmit acoustic waver to media such as human body tissue or water [50–52].

A composite can be modeled by considering its unit cell with infinitesimal dimensions, which is the smallest structure that is periodic in the composite. By changing the volume fraction of the constituents, the shape of the inclusions, or even the topology of the unit cell, we can obtain different effective properties for the composite material [9].

In composite applications, we assume that the excitation wavelengths are so large that the detailed structure of the unit cell does not matter, and the material may be considered as a new homogeneous medium with new effective material properties. Then, the excitation (acoustic, for example) will average out over the fine-scale variations of the composite medium, in the same way as averaging occurs in the micron-sized grain structure in a conventional pure ceramic. When wavelengths are not large enough relative to the size of the unit cell, the composite will present a dispersive behavior with scattering occurring inside the unit cells, making its behavior extremely difficult to model. Homogeneous behavior can be assured by reducing the size of the unit cell relative to the excitation wavelength. However, it is not always possible to guarantee that the size of the microstructure (or unit cell) is smaller than the wavelength.

The homogenization method allows the calculation of effective properties of a complex periodic composite material from its unit cell or microstructure topology, that is, types of constituents and their distribution in the unit cell [53, 54]. This is a general method for calculating effective properties and has no limitations regarding volume fraction or shape of the composite constituents. The main assumptions are that the unit cell is periodic and that the scale of the composite part is much larger than the microstructure dimensions [55–57]. There are other methods that allow calculation of effective properties of a composite material. However, the main advantage of the homogenization technique is that it needs only the information about the unit cell that can have any complex shape. A brief introduction to this method is given in Section 8.6.2.

Assuming that the composite is a homogeneous medium, its behavior can be characterized by Eq. (8.3), by substituting all properties by the effective properties of the composite (or homogenized properties) into these equations [58]. These effective properties can be obtained using the homogenization method presented in Section 8.6.2. Therefore, the constitutive equations of the composite material considering homogenized properties become

$$\begin{cases} \langle \mathbf{T} \rangle = \mathbf{c}_H^E \langle \mathbf{S} \rangle - \mathbf{e}_H \langle \mathbf{E} \rangle \\ \langle \mathbf{D} \rangle = \mathbf{e}_H^t \langle \mathbf{S} \rangle + \boldsymbol{\varepsilon}_H^S \langle \mathbf{E} \rangle \end{cases} \tag{8.38}$$

or

$$\begin{cases} \langle \mathbf{S} \rangle = \mathbf{s}_H^E \langle \mathbf{T} \rangle + \mathbf{d}_H \langle \mathbf{E} \rangle \\ \langle \mathbf{D} \rangle = \mathbf{d}_H^t \langle \mathbf{T} \rangle + \boldsymbol{\varepsilon}_H^T \langle \mathbf{E} \rangle \end{cases} \tag{8.39}$$

where

$$\langle \cdots \rangle = \frac{1}{|V|} \int_V dV \tag{8.40}$$

and the subscript "H" refers to the homogenized properties. $\mathbf{s}_H^E$ is the homogenized compliance tensor under short-circuit conditions, $\boldsymbol{\varepsilon}_H^T$ is the homogenized clamped body dielectric tensor, and $\mathbf{d}_H$ is the homogenized piezoelectric stress tensor. The relations among the properties in Eqs (8.40) and (8.41) are [13]

$$\mathbf{s}^E = \left(\mathbf{c}^E\right)^{-1} \qquad \boldsymbol{\varepsilon}^T = \boldsymbol{\varepsilon}^S + \mathbf{d}^t \left(\mathbf{s}^E\right)^{-1} \mathbf{d} \qquad \mathbf{d} = \left(\mathbf{s}^E\right) \mathbf{e} \tag{8.41}$$

In the following sections, the subscript "H" is omitted for the homogenized properties for the sake of brevity. As a convention, the polarization axis of the piezoelectric material is considered in the third (or z) direction.

8.6.1 Performance Characteristics of Piezocomposite Materials

The main applications of piezocomposites are the generation and detection of acoustic waves. It can be classified as low frequency (hydrostatic operation mode, such as some hydrophones and naval sonars) and high frequency (ultrasonic transducers for imaging). In low-frequency applications, the operation of the device is quasistatic since the operational frequency of the device is generally smaller than the first resonance frequency of the device.

In piezocomposite design, there are several important parameters that directly influence its performance. An ultrasonic transducer, for example, requires a combination of properties such as large piezoelectric coefficient (d_h or g_h, explained below), low density, and mechanical flexibility [59]. However, these properties usually lead to *trade-offs*. To make a flexible ultrasonic transducer, it would be desirable to use the large piezoelectric effects in a poled piezoelectric ceramic; however, ceramics are brittle and stiff, lacking the required flexibility, while polymers having the desired mechanical properties are not piezoelectrics. This problem can be simplified dealing with *figure of merit*, which combines the most sensitive parameters in a form allowing simple comparison of property coefficients. So, the main problem in piezocomposite design is to combine the components in such a manner as to achieve the desired features of each component and also try to maximize the figure of merit [59]. Besides, Newmham *et al.* [59] also studied the connectivity of the individual phases.

The figures of merit that describe the performance of the piezocomposites explained below are obtained by considering only the constitutive properties (neglecting the effects of inertia) as described in Refs [58, 60].

8.6.1.1 Low-Frequency Applications

Consider an orthotropic composite under hydrostatic pressure P as shown in Figure 8.14.

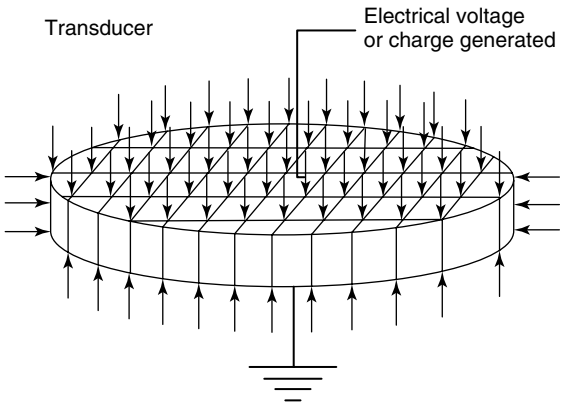

Figure 8.14 Piezocomposite transducer under hydrostatic pressure.

The composite response can be measured by three different quantities [61]:

- **Hydrostatic coupling coefficient (d_h)**:

$$d_h = \frac{\langle \mathbf{D}_3 \rangle}{P} = d_{33} + d_{23} + d_{13} \tag{8.42}$$

- **Figure of merit ($d_h g_h$)**:

$$g_h = \frac{\langle E_3 \rangle}{P} = \frac{d_h}{\varepsilon_{33}^T} \Rightarrow d_h g_h = \frac{d_h^2}{\varepsilon_{33}^T} \tag{8.43}$$

- **Hydrostatic electromechanical coupling factor (k_h)**:

$$k_h = \sqrt{\frac{d_h^2}{\varepsilon_{33}^T s_h^E}} \tag{8.44}$$

where $s_h = (\langle \varepsilon_1 \rangle + \langle \varepsilon_2 \rangle + \langle \varepsilon_3 \rangle)/P$ is the dilatational compliance. For an orthotropic material, $s_h^E = s_{11}^E + s_{22}^E + s_{33}^E + s_{12}^E + s_{13}^E + s_{23}^E$, and the coefficients s_{kl}^E are those defined in Eq. (8.39).

The quantities d_h and g_h measure the response of the material in terms of electrical charge and electrical voltage generated, respectively, when subjected to a hydrostatic pressure field considering a null electric field ($\langle E_3 \rangle = 0$, for short-circuit conditions) and null electric displacement ($\langle D_3 \rangle = 0$, for open circuit conditions), respectively. $d_h g_h$ is the product of d_h and g_h. The coefficient k_h measures the overall acoustic/electric power conversion. The expressions for d_h and s_h^E can be obtained by substituting the hydrostatic pressure into Eq. (8.39) and considering a null electric field ($\langle E_3 \rangle = 0$). The expression for g_h can be obtained in the same way, but considering null electric displacement ($\langle D_3 \rangle = 0$) in Eq. (8.39).

These quantities can be written in terms of the properties described in Eq. (8.38) by using Eq. (8.41). The definitions presented above consider an orthotropic piezocomposite material. If a transversely isotropic composite in the 12 (or $x\gamma$) plane is considered, then $s_{13}^E = s_{23}^E$, $s_{11}^E = s_{22}^E$, and $d_{13} = d_{23}$.

8.6.1.2 High-Frequency Applications

In ultrasonic applications, thin plates of the piezocomposite are excited near their thickness-mode resonance. In this case, the quantity that describes the performance of the ultrasonic transducer is given by Smith and Auld [60]:

- **Electromechanical coupling factor (k_t)**

$$k_t = \sqrt{\frac{e_{33}^2}{c_{33}^D \varepsilon_{33}^S}} \tag{8.45}$$

where the properties are the same as defined in Eq. (8.38) and $c_{33}^D = c_{33}^E + (e_{33})^2/\varepsilon_{33}^S$.

8.6.2 Homogenization Method

The homogenization method was initially developed to solve partial differential equations whose parameters vary rapidly in space. In engineering field, this method has been used to obtain effective properties of composite materials [62], allowing us to save the effort. For example, imagine a perforated beam as illustrated in Figure 8.15a. If we were to build an FEM model of the beam by considering all the holes, it would be very difficult to model and the computational cost would be prohibitive. However, it can be understood as a continuous beam (no holes) made of a material with properties equal to the effective properties of a ''composite'' material whose unit cell consists of a square with a circular hole inside, that is, a homogenized material. Therefore, if we have the effective properties of this composite material, the beam can be modeled as a homogeneous medium by building a simple FEM model with corresponding homogenized properties.

The same concept can be applied to model a wall made of bricks, for example, as illustrated in Figure 8.15b; however, it is important to mention that the

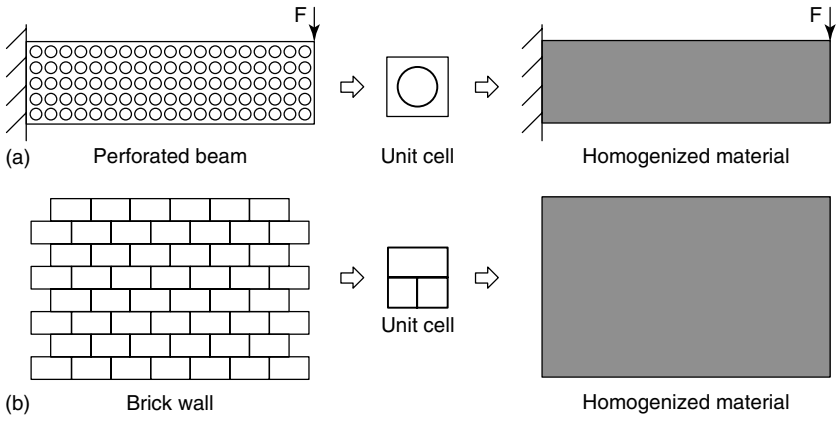

Figure 8.15 Homogenization concept: (a) perforated beam and (b) brick wall.

size of phenomenon we are interested in analyzing will determine whether homogenization concept can be applied. The wall can be understood as a composite material, whose unit cell is described in Figure 8.15b. In another case, suppose that we want to model a bullet hitting the wall. If the bullet size is much larger than the unit cell size, homogenization can be applied and the entire wall can be modeled as a homogeneous material with corresponding effective properties. However, if the bullet size is of the same order of wall unit cell size (i.e., the brick), then homogenization cannot be applied and a detailed FEM model of the wall must be built taking into account the unit cell details.

Homogenization equations are obtained by first expanding displacement **u** in zeroth-order and first-order terms. The zeroth-order terms represent the ''average'' values of displacement over the piezocomposite domain scale (**x**), while the first-order terms represent the variation of displacement in the unit cell domain scale (**y**), that is,

$$\mathbf{u}^{\varepsilon} = \mathbf{u}_0(\mathbf{x}) + \varepsilon \mathbf{u}_1(\mathbf{x}, \mathbf{y}) \tag{8.46}$$

where ε is a small number. This expression is substituted in the energy formulation for the medium and, by using variational calculus, the so-called homogenization equations related only to the **y** scale are extracted. Essentially, the meaning of homogenization equations consists in applying different load cases to the unit cell to calculate its response to these load cases. On the basis of these responses, the composite effective properties are obtained. Since the unit cell may have a complex shape, these equations are solved by using FEM.

The basic homogenization equations applied to calculate the effective properties of elastic materials are presented below:

$$\frac{1}{|Y|}\int_Y \left[c_{ijkl}(\mathbf{x}, \mathbf{y}) \left(\delta_{im}\delta_{jn} + \frac{\partial \chi_i^{(mn)}}{\partial y_j} \right) \right] S_{kl}(\mathbf{v})\, dY = 0 \qquad \forall \mathbf{v} \in H_{\text{per}}\left(Y, R^3\right) \tag{8.47}$$

$$H_{\text{per}}\left(Y, R^3\right) = \{\mathbf{v} = (v_i) \,|v_i \in H_1(Y),\ i = 1, 2, 3\}$$

$$H_{\text{per}}(Y) = \left\{\mathbf{v} \in H_1(Y) \,|\mathbf{v} \text{ takes equal values on opposite sides of Y}\right\}$$

This homogenization formulation has no limitations regarding volume fraction or the shape of the composite constituents, and is based upon assumptions of periodicity of the microstructure and the separation of the microstructure scale from the component scale through an asymptotic expansion.

Now consider a composite material under dynamic excitation (electrical or mechanical). If the operational wavelength is larger than the unit cell dimensions, it seems natural that homogenization equations can be applied. This situation is called a *static case*. If operational wavelength is smaller than the unit cell dimensions, then unit cell scale will affect the calculation of effective properties, that is, the effective properties will have a dispersive behavior as before. Essentially, what happens is that if the wavelength is smaller than unit cell dimensions, there will be wave reflections inside of the unit cell and this effect must be taken into account in the homogenization equations. This situation is called a *dynamic case*

and homogenization equations must be developed again, originating the so-called homogenization equations for the dynamic case.

For a piezoelectric medium, the homogenization theory for piezoelectricity considering the static case (where the operational wavelength is much larger than the unit cell dimensions) was developed by Telega [63]. Galka *et al.* [64] present the homogenization equations and effective properties for thermopiezoelectricity considering the static case. For dynamic applications (wavelength is of the same size as, or smaller than, the unit cell dimensions), Turbé and Maugin [65] developed a homogenization formulation to obtain the dynamical effective properties of the piezoelectric medium. In the limit of the static (and low-frequency) case, they recovered the expressions derived by Telega [63]. Finally, Otero *et al.* [66] developed general homogenized equations and effective properties for (heterogeneous and periodic) piezoelectric medium by considering terms of infinite order in the homogenization asymptotic expansion.

The homogenization equations for piezoelectric medium considering the static case are [63]

$$\begin{aligned}
&\frac{1}{|Y|}\int_Y \left[c^E_{ijkl}\left(\mathbf{x},\mathbf{y}\right)\left(\delta_{im}\delta_{jn}+\frac{\partial \chi_i^{(mn)}}{\partial y_j}\right)+e_{ikl}\left(\mathbf{x},\mathbf{y}\right)\frac{\partial \psi^{(mn)}}{\partial y_i}\right] S_{kl}\left(\mathbf{v}\right)dY=0\\
&\forall \mathbf{v}\in H_{\text{per}}\left(Y,R^3\right)\\
&\frac{1}{|Y|}\int_Y \left[e_{ikl}\left(\mathbf{x},\mathbf{y}\right)\left(\delta_{im}\delta_{jn}+\frac{\partial \chi_i^{(mn)}}{\partial y_j}\right)-\varepsilon^S_{ik}\left(\mathbf{x},\mathbf{y}\right)\frac{\partial \psi^{(mn)}}{\partial y_i}\right]\frac{\partial \varphi}{\partial y_k}dY=0\\
&\forall \varphi\in H_{\text{per}}\left(Y\right)
\end{aligned} \tag{8.48}$$

and

$$\begin{aligned}
&\frac{1}{|Y|}\int_Y \left[c^E_{klij}\left(\mathbf{x},\mathbf{y}\right)\frac{\partial \Phi_k^{(m)}}{\partial y_l}+e_{kij}\left(\mathbf{x},\mathbf{y}\right)\left(\delta_{mk}+\frac{\partial R^{(m)}}{\partial y_k}\right)\right] S_{ij}\left(\mathbf{v}\right)dY=0\\
&\forall \mathbf{v}\in H_{\text{per}}\left(Y,R^3\right)\\
&\frac{1}{|Y|}\int_Y \left[e_{kij}\left(\mathbf{x},\mathbf{y}\right)\frac{\partial \Phi_i^{(m)}}{\partial y_j}-\varepsilon^S_{ik}\left(\mathbf{x},\mathbf{y}\right)\left(\delta_{mi}+\frac{\partial R^{(m)}}{\partial y_i}\right)\right]\frac{\partial \varphi}{\partial y_k}dY=0\\
&\forall \varphi\in H_{\text{per}}\left(Y\right)
\end{aligned} \tag{8.49}$$

These equations are equivalent to Eq. (8.47) for elastic medium. They are obtained by expanding piezocomposite displacement $\mathbf{u}$ and electrical potential ϕ in zeroth-order and first-order terms. The zeroth-order terms represent the "average" values of these quantities over the piezocomposite domain scale $(\mathbf{x})$, while first-order terms represent the variation of these quantities in the unit cell domain scale $(\mathbf{y})$, that is,

$$\begin{aligned}
\mathbf{u}^{\varepsilon} &= \mathbf{u}_0\left(\mathbf{x}\right)+\varepsilon\mathbf{u}_1\left(\mathbf{x},\mathbf{y}\right)\\
\phi^{\varepsilon} &= \phi_0\left(\mathbf{x}\right)+\varepsilon\phi_1\left(\mathbf{x},\mathbf{y}\right)
\end{aligned} \tag{8.50}$$

The characteristic functions χ_i, ψ, Φ_i, R represent the displacement and electrical response of the unit cell to the applied load cases (Figure 8.17).

By using FEM formulation to solve Eqs (8.48) and (8.49), the following matrix system is obtained [67]:

$$\begin{bmatrix} \mathbf{K_{uu}} & \mathbf{K_{u\phi}} \\ \mathbf{K}_{\mathbf{u}\phi}^{t} & -\mathbf{K}_{\phi\phi} \end{bmatrix} \begin{Bmatrix} \hat{\chi}^{(mn)} \\ \hat{\psi}^{(mn)} \end{Bmatrix} = \begin{Bmatrix} \mathbf{F}^{(mn)} \\ \mathbf{Q}^{(mn)} \end{Bmatrix}$$
$$\begin{bmatrix} \mathbf{K_{uu}} & \mathbf{K_{u\phi}} \\ \mathbf{K}_{\mathbf{u}\phi}^{t} & -\mathbf{K}_{\phi\phi} \end{bmatrix} \begin{Bmatrix} \hat{\Phi}^{(mn)} \\ \hat{R}^{(mn)} \end{Bmatrix} = \begin{Bmatrix} \mathbf{F}^{(mn)} \\ \mathbf{Q}^{(mn)} \end{Bmatrix} \tag{8.51}$$

where $\hat{\chi}$, $\hat{\psi}$, $\hat{\Phi}$, $\hat{R}$ are the corresponding nodal values of the characteristics functions χ_i, ψ, Φ_i, R respectively, and

$$F_{iI}^{e(mn)} = -\int_{\Omega^e} c_{ijmn}^{E} \frac{\partial N_I}{\partial y_j} d\Omega^e \quad Q_I^{e(mn)} = -\int_{\Omega^e} e_{kmn} \frac{\partial N_I}{\partial y_k} d\Omega^e$$
$$F_{iI}^{e(m)} = -\int_{\Omega^e} e_{mij} \frac{\partial N_I}{\partial y_j} d\Omega^e \quad Q_I^{e(m)} = -\int_{\Omega^e} \varepsilon_{mj}^{S} \frac{\partial N_I}{\partial y_j} d\Omega^e \tag{8.52}$$

The other terms are defined in Section 8.4.2. By analyzing Eq. (8.52) we conclude that for the three-dimensional problem, there are nine load cases to be solved independently. Six of them come from Eq. (8.48), where the indices m and n can be 1, 2, or 3, resulting in the following mn combinations: 11, 22, 33, 12 or 21, 23 or 32, and 13 or 31. The remaining three load cases come from Eq. (8.49) where the index m can be 1, 2, and 3. For example, in the two-dimensional problem, there are five load cases to be solved independently (Figure 8.17). Three of them come from Eq. (8.48), where the indices m and n can be 1 or 3, resulting in the combinations 11, 33, and 13 or 31, for mn. The other two load cases come from Eq. (8.49) where the index m can be 1 or 3. All load cases must be solved by enforcing periodic boundary conditions in the unit cell for the displacements and electrical potentials. The displacements and electrical potential of some point of the cell must be prescribed to overcome the nonunique solution of the problem; otherwise, the problem will be ill posed [68]. The choice of the point of the prescribed values does not affect the homogenized coefficients since only derivatives of the characteristic functions are used for their computation. The numerical solution of matrix system (Eq. (8.52)) has already been discussed in Section 8.4.2.

The applied load cases for the bidimensional problem considering elastic material (Eq. (8.47)) and piezoelectric material (Eqs (8.48) and (8.49)) are described in Figures 8.16 and 8.17, respectively.

After solving for the characteristic displacements and electrical potentials, the effective properties are computed by using Eq. (8.53):

$$c_{pqrs}^{H}(\mathbf{x}) = \frac{1}{|Y|}\int_Y \left[c_{pqrs}^{E}(\mathbf{x},\mathbf{y}) + c_{pqkl}^{E}(\mathbf{x},\mathbf{y}) \frac{\partial \chi_k^{(m)}}{\partial y_l} + e_{kpq}(\mathbf{x},\mathbf{y}) \frac{\partial \psi^{(rs)}}{\partial y_k} \right] dY$$
$$e_{prs}^{H}(\mathbf{x}) = \frac{1}{|Y|}\int_Y \left[e_{prs}(\mathbf{x},\mathbf{y}) + e_{pij}(\mathbf{x},\mathbf{y}) \frac{\partial \chi_i^{(rs)}}{\partial y_j} - \varepsilon_{pk}^{S}(\mathbf{x},\mathbf{y}) \frac{\partial \psi^{(rs)}}{\partial y_k} \right] dY$$
$$\varepsilon_{pq}^{H}(\mathbf{x}) = \frac{1}{|Y|}\int_Y \left[\varepsilon_{pq}^{S}(\mathbf{x},\mathbf{y}) + \varepsilon_{pj}^{S}(\mathbf{x},\mathbf{y}) \frac{\partial R^{(q)}}{\partial y_j} - e_{pij}(\mathbf{x},\mathbf{y}) \frac{\partial \Phi_i^{(q)}}{\partial y_j} \right] dY \tag{8.53}$$

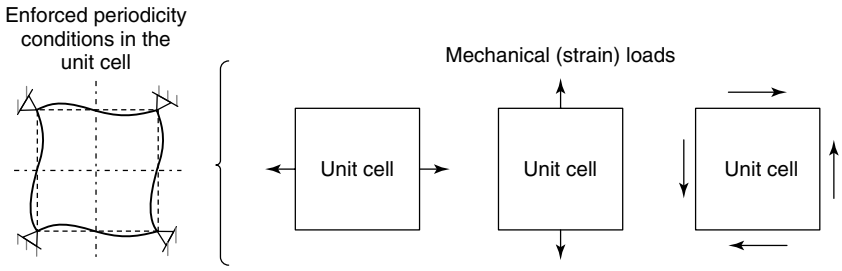

Figure 8.16 Load cases for homogenization of elastic materials.

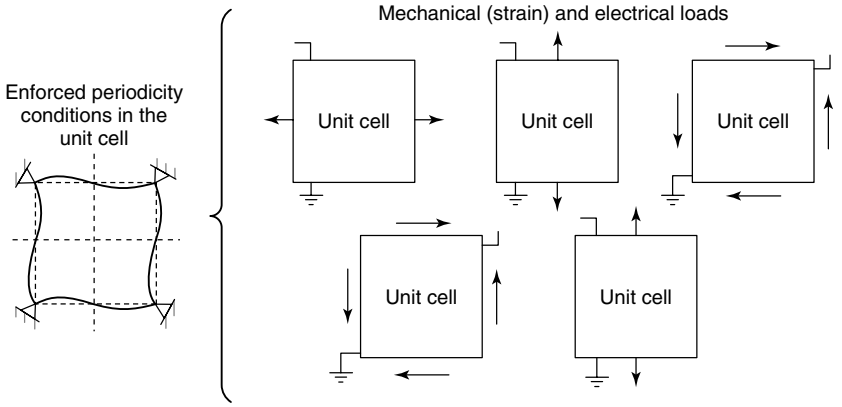

Figure 8.17 Load cases for homogenization of piezoelectric materials.

The concept of the continuum distribution of design variable based on the CAMD method discussed in Section 8.5.2 is also considered here.

8.6.3 Examples

Of the currently available configurations, the 2–2 piezocomposite has been the focus of most studies, which consists of alternating layers of piezoceramic PZT and polymer as shown in Figure 8.18. To illustrate the FGM concept for piezoelectricity, the results of calculated effective properties for 2–2 piezocomposite are presented.

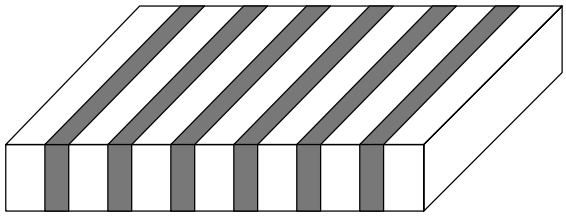

Figure 8.18 2–2 piezocomposite.

Table 8.1 Material properties.

Properties		PZT-5A	Epoxy polymer
Dielectric properties (F m^{-1})	ε_0	8.85×10^{-12}	8.85×10^{-12}
	ε_{11}^S	$916 \times \varepsilon_0$	$3.6 \times \varepsilon_0$
	ε_{33}^S	$830 \times \varepsilon_0$	$3.6 \times \varepsilon_0$
Piezoelectric properties (C m^{-2})	e_{31}	−5.4	0.0
	e_{33}	15.8	0.0
	e_{15}	12.3	0.0
Elastic properties (N m^{-2})	C_{11}^E	12.1×10^{10}	9.34×10^9
	C_{12}^E	7.54×10^{10}	9.34×10^9
	C_{13}^E	7.52×10^{10}	9.34×10^9
	C_{33}^E	11.1×10^{10}	9.34×10^9
	C_{44}^E	2.11×10^{10}	9.34×10^9
	C_{66}^E	2.28×10^{10}	9.34×10^9
Density (kg m^{-3})		7500	1340

Here, ''2–2'' designates the connectivity of the piezocomposite material; however, many other connectivities, such as 3−1 and 1−1, are also possible [59]. The example considers a bidimensional model (plane strain) of a 2–2 piezocomposite made of PZT-5A/ Epoxy (Table 8.1). The ''volume fraction'' (vol%) was set to 20% of PZT-5A, located in a vertical line in the middle, and 80% of epoxy polymer, distributed in the rest of the unit cell. Three cases are considered: a non-FGM unit cell and two FGM unit cells, with linear and sinusoidal gradations. These three cases are compared with the full unit cell of PZT-5A, in order to quantify the effects of the FGM on the performance characteristics.

Figures 8.19–8.21 show the graphics of the PZT-5A distribution in the *x* direction, where 1 refers to pure PZT-5A and 0 refers to pure epoxy polymer. The images in the (b) show the distributed material in the unit cell, where the PZT-5A is

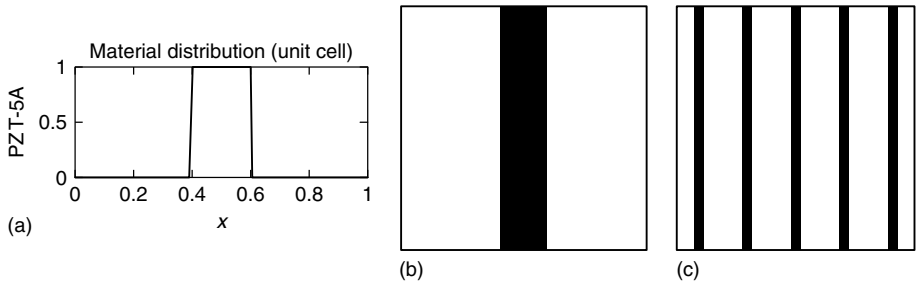

Figure 8.19 Non-FGM 2–2 piezocomposite. (a) Material distribution graphic of PZT-5A; (b) unit cell; and (c) periodic array.

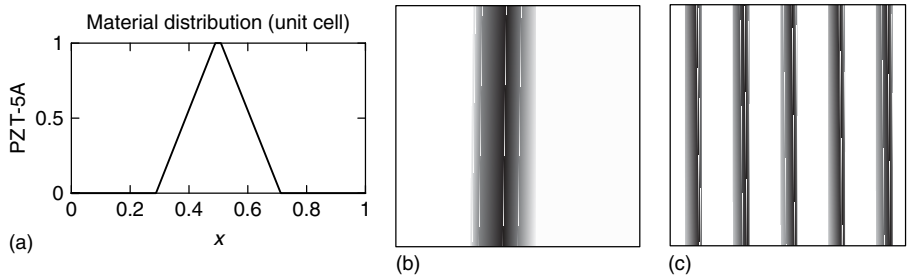

Figure 8.20 Linear FGM 2–2 piezocomposite. (a) Material distribution graphic of PZT-5A; (b) unit cell; and (c) periodic array.

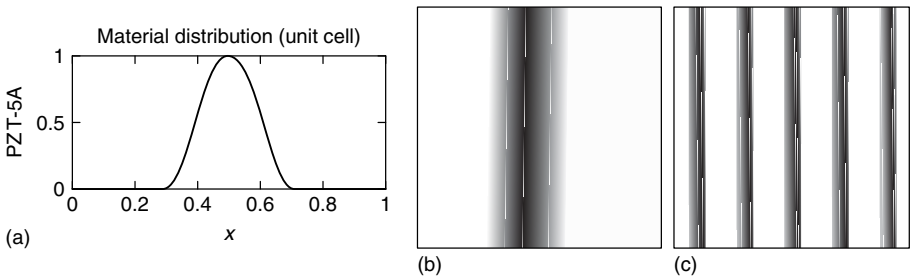

Figure 8.21 Sinusoidal FGM 2–2 piezocomposite. (a) Material distribution graphic of PZT-5A; (b) unit cell; and (c) periodic array.

represented as black and epoxy as white. The images (c) of these figures represent the periodic array of the unit cells.

Table 8.2 presents the performance characteristics for each type of unit cell. From Table 8.2, it is noticed that each performance characteristic is maximized by using different topologies of the unit cell. Considering the four topologies analyzed here, the topology that maximizes d_h and k_t is the traditional non-FGM 2-2 piezocomposite (Figure 8.19). However, $d_h g_h$ is maximized by using the linear or sinusoidal 2-2 piezocomposite (Figures 8.20 and 8.21, respectively). This fact indicates that it is possible to achieve higher performance characteristics by using 20% of PZT-5A in the unit cell distributed in a functionally graded way. The advantages, in addition to better performance of the piezocomposite, are the weight reduction and cost savings in the final material, as the epoxy polymer is lighter and chapter than the PZT-5A ceramic. the exception is k_h, which is maximized by using the pure PZT-5A material. However, the linear and sinusoidal 2-2 piezocomposite present a near value of k_h (0.177 and 0.122, respectively) and a lighter density (3496 kg/m^3) than the pure PZT-5A ceramic material (7500 kg/m^3) because the density of epoxy polymer is 56 times lighter then PZT-5A (see Table 8.1). Therefore, there is a trade off in choosing the topology of the unit cell among performance, weight and, consequently, cost in the final application. This trade off is also noticed in the performance characteristics d_h and k_t.

Table 8.2 Performance characteristics of the unit cells.

Material distribution	Density (kg/m^3)	Low-frequency applications			High-frequency applications
		d_h(pC/N)	$d_h g_h$(pm^2/N)	k_h	k_t
100% PZT-5A (full)	7500	68.196	0.222	0.145	0.361
Figure 8.19	3496	92.536	1.038	0.092	0.477
Figure 8.20	3496	73.804	1.700	0.117	0.422
Figure 8.21	3496	80.864	1.584	0.112	0.443

From these results, it is possible to conclude that FGM concept can be applied to obtain materials with the same or even higher properties of regular materials with weight reduction. Also the choice of the function applied for gradation has an important role in the design of the unit cells. The design of FGM unit cells is not trivial and requires optimization tools to avoid trial-and-error approaches.

8.7 Conclusion

The results give an idea about the potential of applying the FGM concept to design smart materials, both in micro- and macroscales. It is observed that piezoelectric transducers, designed according to FGM concept, have improved their performance in relation to nongraded ones; for instance, in ultrasonic applications, the FGM concept allows designing piezoelectric transducer with small time waveform or large bandwidth, which is desirable for obtaining high imaging resolution for medical and nondestructive testing applications. Likewise, it is observed that when the unit cell of 2–2 piezocomposite is designed on the basis of the FGM concept, high values of d_h, $d_h g_h$, and k_h are achieved, while the density value is significantly reduced in relation to the nongraded unit cell, which is desirable in applications to hydrophones. Additionally, from the examples, it is clear that both in micro- and macroscales the gradation function defines the piezoelectric behavior and, hence, optimization techniques must be used for designing graded piezoelectric structures. Specifically, the TOM arises as a general and powerful approach to find the optimal gradation function for achieving user-defined goals. In conclusion, the practical use of the proposed approach (to design piezoelectric structures considering gradation in micro- and macroscales) can broaden the range of application in the field of smart structures.

Acknowledgments

Wilfredo Montealegre Rubio and Sandro Luis Vatanabe thank FAPESP (São Paulo State Foundation Research Agency) for supporting them in their graduate studies

through the fellowship No. 05/01762-5 and No. 08/57086-6, respectively. Emílio Carlos Nelli Silva is thankful for the financial support received from both CNPq (National Council for Research and Development, Brazil, No. 303689/2009-9). Gláucio H. Paulino acknowledges FAPESP for providing him the visiting scientist award at the University of São Paulo (USP) through project number 2008/5070-0.

References

1. Miyamoto, Y., Kaysser, W.A., Rabin, B.H., Kawasaki, A., and Ford, R.G. (1999) *Functionally Graded Materials: Design, Processing and Applications*, Kluwer Academic Publishers, London.
2. Suresh, S. and Mortensen, A. (1988) *Fundamentals of Functionally Graded Materials*, IOM Communications, London.
3. Paulino, G.H., Jin, Z.-H., and Dodds, R.H. Jr. (2003) Failure of functionally graded materials. *Comprehensive Structural Integrity*, **2**, 607–644.
4. Yamada, K., Sakamura, J.-I., and Nakamura, K. (1998) Broadband ultrasound transducers using effectively graded piezoelectric materials. IEEE Ultrasonics Symposium, pp. 1085–1089.
5. Samadhiya, R. and Mukherjee, A. (2006) Functionally graded piezoceramic ultrasonic transducers. *Smart Materials and Structures*, **15** (6), 627–631.
6. Chakraborty, A., Gopalakrishnan, S., and Kausel, E. (2005) Wave propagation analysis in inhomogeneous piezo-composite layer by the thin layer method. *International Journal for Numerical Methods in Engineering*, **64** (5), 567–598.
7. Guo, H., Cannata, J., Zhou, Q., and Shung, K. (2005) Design and fabrication of broadband graded ultrasonic transducers with rectangular kerfs. *IEEE Transaction on Ultrasonics, Ferroelectrics, and frequency Control*, **52** (11), 2096–2102.
8. Ichinose, N., Miyamoto, N., and Takahashi, S. (2004) Ultrasonic transducers with functionally graded piezoelectric ceramics. *Journal of the European Ceramic Society*, **24**, 1681–1685.
9. Torquato, S. (2002) *Random Heterogeneous Materials – Microstructure and Macroscopic Properties*, Springer, New York, ISBN-10:0387951679.
10. Ikeda, T. (1996) *Fundamentals of Piezoelectricity*, Oxford University Press, Oxford.
11. Nye, J.F. (1993) *Physical Properties of Crystals: Their Representation by Tensors and Matrices*, Clarendon Press, Oxford.
12. Kino, G. (2000) *Acoustic Waves: Devices, Imaging, and Analog Signal Processing*, Corrected Edition, Prentice-Hall, Inc., New Jersey.
13. ANSI/IEEE (1996) Publication and proposed revision of ANSI/IEEE standard 176-1987 ''ANSI/IEEE Standard on Piezoelectricity''. *IEEE Transactions on Ultrasonics, Ferroelectrics, and Frequency Control*, **43** (5), 717–772.
14. Naillon, M., Coursant, R.H., and Besnier, F. (1983) Analysis of piezoelectric structures by a finite element method. *Acta Electronica*, **25** (4), 341–362.
15. Kieback, B., Neubrand, A., and Riedel, H. (2003) Processing techniques for functionally graded materials. *Materials Science and Engineering: A*, **362**, 81–105.
16. Yin, H.M., Sun, L.Z., and Paulino, G.H. (2004) Micromechanics-based elastic model for functionally graded materials with particle interactions. *Acta Marterialia*, **52** (12), 3535–3543.
17. Koizumi, M. (1997) FGM activities in Japan. *Composites Part B: Engineering*, **28** (1), 1–4.
18. Birman, V. and Byrd, W.L. (2007) Modeling and analysis of functionally graded materials and structures. *Applied Mechanical Review*, **60** (5), 195–216.
19. Qiu, J.H., Tani, J., Ueno, T., Morita, T., Takahashi, H., and Du, H.J. (2003) Fabrication and high durability of functionally graded piezoelectric bending actuators. *Smart Materials and Structures*, **12** (1), 115–121.

20. Huang, J. and Rapoff, A.J. (2003) Optimization design of plates with holes by mimicking bones through non-axisymmetric functionally graded material. *Journal of Materials: Design and Applications*, **217** (1), 23–27.
21. Hedia, H.S. (2005) Comparison of one-dimensional and two-dimensional functionally graded materials for the backing shell of the cemented acetabular cup. *Journal of Biomedical Materials Research Part B: Applied Biomaterials*, **74B** (2), 732–739.
22. Huang, M., Wang, R., Thompson, V., Rekow, D., and Soboyejo, W. (2007) Bioinspired design of dental multilayers. *Journal of Material Science: Materials in Medicine*, **18** (1), 57–64.
23. Silva, E.C.N., Walters, M.C., and Paulino, G.H. (2006) Modeling bamboo as a functionally graded material: Lessons for the analysis of affordable materials. *Journal of Materials Science*, **41**, 6991–7004.
24. Lee, W.Y., Stinton, D.P., Berndt, C.C., Erdogan, F., Lee, Y.D., and Mutasim, Z. (1996) Concept of functionally graded materials for advanced thermal barrier coating applications. *Journal of the American Ceramic Society*, **79** (12), 3003–3012.
25. Pompe, W., Worch, H., Epple, M., Friess, W., Gelinsky, M., Greil, P., Hempel, U., Scharnweber, D., and Schulte, K. (2003) Functionally graded materials for biomedical applications. *Materials Science and Engineering: A*, **362** (1–2), 40–60.
26. Almajid, A., Taya, M., and Hudnut, S. (2001) Analysis of out-of-plane displacement and stress field in a piezocomposite plate with functionally graded microstructure. *International Journal of Solids and Structures*, **38** (19), 3377–3391.
27. Shi, Z.F. and Chen, Y. (2004) Functionally graded piezoelectric cantilever beam under load. *Archive of Applied Mechanics*, **74**, 237–247.
28. Taya, M., Almajid, A.A., Dunn, M., and Takahashi, H. (2003) Design of bimorph piezocomposite actuators with functionally graded microstructure. *Sensors and Actuators A-Physical*, **107** (3), 248–260.
29. Zhu, X.H. and Meng, Z.Y. (1995) Operational principle, fabrication and displacement characteristics of a functionally gradient piezoelectric ceramic actuator. *Sensors and Actuators A-Physical*, **48** (3), 169–176.
30. Rubio, W.M., Buiochi, F., Adamowski, J.C., and Silva, E.C.N. (2009) Modeling of functionally graded piezoelectric ultrasonic transducers. *Ultrasonics*, **49** (4-5), 484–494.
31. Wang, B.L. and Noda, N. (2001) Design of a smart functionally graded thermopiezoelectric composite structure. *Smart Materials and Structures*, **10** (2), 189–193.
32. Krautkramer, J. and Krautkramer, H. (1977) *Ultrasonic Testing of Materials*, 2nd edn, Springer-Verlag, New York.
33. Tiersten, H.F. (1967) Hamilton's principle for linear piezoelectric media. *Proceedings of the IEEE*, **55** (8), 1523–1524.
34. Zienkiewicz, O.C. and Taylor, R.L. (1991) *The Finite Element Method*, 4th edn, McGraw-Hill, New York.
35. Zuiker, J. and Dvorak, G. (1994) The effective properties of functionally graded composites-I. Extension of Mori-Tanaka method to linearly varying fields. *Composite Engineering*, **4** (1), 19–35.
36. Kim, J.H. and Paulino, G.H. (2002) Isoparametric graded finite elements for nonhomogeneous isotropic and orthotropic materials. *Journal of Applied Mechanics: Transactions of the ASME*, **69** (4), 502–514.
37. Silva, E.C.N., Carbonari, R.C., and Paulino, G.H. (2007) On graded elements for multiphysics applications. *Smart Materials and Structures*, **16**, 2408–2428.
38. Mills, D. and Smith, S.W. (2002) Multi-layered PZT/polymer composites to increase signal-to-noise ratio and resolution for medical ultrasound transducers part II: thick film technology. *IEEE Transactions on Ultrasonics, Ferroelectrics and Frequency Control*, **49** (7), 1005–1014.
39. Lamberti, N., Caliano, G., Iula, A., and Pappalardo, M. (1997) A new approach for the design of ultrasono-therapy

transducers. *IEEE Transactions on Ultrasonics, Ferroelectrics and Frequency Control*, **44** (1), 77–84.

40. Ludwig, G.D. (1950) The velocity of sound through tissues and the acoustic impedance of tissues. *The Journal of the Acoustical Society of America*, **22** (6), 862–866.
41. Rubio, W.M., Silva, E.C.N., and Paulino, G.H. (2009) Toward optimal design of piezoelectric transducers based on multifunctional and smoothly graded hybrid material systems. *Journal of Intelligent Material Systems and Structures*, **20** (14), 1725–1746.
42. Carbonari, R.C., Silva, E.C.N., and Paulino, G.H. (2009) Multi-actuated functionally graded piezoelectric micro-tools design: A multiphysics topology optimization approach. *International Journal for Numerical Methods in Engineering*, **77** (3), 301–336.
43. Carbonari, R.C., Silva, E.C.N., and Paulino, G.H. (2007) Topology optimization design of functionally graded bimorph-type piezoelectric actuators. *Smart Materials and Structures*, **16** (6), 2607–2620.
44. Bendsøe, M.P. and Sigmund, O. (2003) *Topology Optimization: Theory, Methods and Applications*, Springer, Berlin.
45. Rubio, W.M., Buiochi, F., Adamowski, J.C., and Silva, E.C.N. (2010) Topology optimized design of functionally graded piezoelectric ultrasonic transducers. *Physics Procedia*, **3** (1), 891–896.
46. Guo, N., Cawley, P., and Hitchings, D. (1992) The finite element analysis of the vibration characteristics of piezoelectric discs. *Journal of Sound and Vibration*, **159** (1), 115–138.
47. Kim, T.S. and Kim, Y.Y. (2000) MAC-based mode-tracking in structural topology optimization. *Computers and Structures*, **74** (3), 375–383.
48. Matsui, K. and Terada, K. (2004) Continuous approximation of material distribution for topology optimization. *International Journal for Numerical Methods in Engineering*, **59** (14), 1925–1944.
49. Guest, J.M., Prevost, J.H., and Belytschko, T. (2004) Achieving minimum length scale in topology optimization using nodal design variables and projection functions. *International Journal for Numerical Methods in Engineering*, **61** (2), 238–254.
50. Smith, W.A. (1989) The role of piezocomposites in ultrasonic transducers. Proceedings of IEEE Ultrasonic Symposium, pp. 755–765.
51. Smith, W.A. (1990) The application of 1–3 piezocomposites in acoustic transducers. Proceedings of 7th International Symposium on Applications of Ferroelectrics, pp. 145–152.
52. Safari, A. (1994) Development of piezoelectric composites for transducers. *Journal de Physique III*, **4** (7), 1129–1149.
53. Sanchez-Palencia, E. (1980). *Non-Homogeneous Media and Vibration Theory*, Lectures Notes in Physics, vol. 127, Springer, Berlin.
54. Guedes, J.M. and Kikuchi, N. (1990) Preprocessing and postprocessing for materials based on the homogenization method with adaptive finite element methods. *Computer Methods in Applied Mechanics and Engineering*, **83**, 143–198.
55. Cherkaev, A. and Kohn, R. (1997) *Topics in the Mathematical Modeling of Composite Materials*, Birkhauser, Boston, ISBN-10: 3764336625.
56. Allaire, G. (2002) *Shape Optimization by the Homogenization Method*, Applied Mathematical Sciences, vol. 146, Springer, New York, ISBN-10: 0387952985.
57. Guedes, J.M. and Kikuchi, N. (1990) Preprocessing and postprocessing for materials based on the homogenization method with adaptive finite-element methods. *Computer Methods in Applied Mechanics and Engineering*, **83** (2), 143–198.
58. Smith, W.A. (1993) Modeling 1-3 composite piezoelectrics: hydrostatic response. *IEEE Transactions on Ultrasonics, Ferroelectrics, and Frequency Contrl.*, **40** (1), 41–49.
59. Newnham, R.E., Skinner, D.P., and Cross, L.E. (1978) Connectivity and piezoelectric-pyroelectric composites. *Materials Research Bulletin*, **13** (5), 525–536.
60. Smith, W.A. and Auld, B.A. (1991) Modeling 1-3 composite piezoelectrics:

thickness-mode oscillations. *IEEE Transactions on Ultrasonics, Ferroelectrics, and Frequency Control*, **38** (1), 40–47.

61. Avellaneda, M. and Swart, P.J. (1994) The role of matrix porosity and poisson's ratio in the design of high-sensitivity piezocomposite transducers. *Adaptive Structures and Composites Materials: Analysis and Application – ASME Aerospace Division AD*, **45**, 59–66.

62. Sanchez-Palencia, E. and Zaoui, A. (1985) *Homogenization Techniques for Composite Media*, Lecture Notes in Physics, Springer-Verlag.

63. Telega, J.J. (1990) Piezoelectricity and homogenization: application to biomechanics. *Continuum Models and Discrete Systems*, **2**, 220–230.

64. Galka, A., Telega, J.J., and Wojnar, R. (1992) Homogenization and thermopiezoelectricity. *Mechanics Research Communications*, **19** (4), 315–324.

65. Turbé, N. and Maugin, G.A. (1991) On the linear piezoelectricity of composite materials. *Mathematical Methods in the Applied Sciences*, **14** (6), 403–412.

66. Otero, J.A., Catillero, J.B., and Ramos, R.R. (1997) Homogenization of heterogeneous piezoelectric medium. *Mechanics Research Communications*, **24** (1), 75–84.

67. Silva, E.C.N., Fonseca, J.S.O., and Kikuchi, N. (1997) Optimal design of piezoelectric microstructures. *Computational Mechanics*, **19** (5), 3987–3410.

68. Silva, E.C.N., Fonseca, J.S.O., and Kikuchi, N. (1998) Optimal design of periodic piezocomposites. *Computer Methods in Applied Mechanics and Engineering*, **159**, 49–77.